THE ASTROPHYSICAL JOURNAL, 526:890–915, 1999 December 1

THE LICK PLANET SEARCH: DETECTABILITY AND MASS THRESHOLDS

ANDREW CUMMING,[1,2] GEOFFREY W. MARCY,[2,3] AND R. PAUL BUTLER[4]

Received 1999 February 9; accepted 1999 July 15

ABSTRACT

We present an analysis of 11 yr of precision radial velocity measurements of 76 nearby solar-type stars from the Lick radial velocity survey. For each star, we report on variability, periodicity, and long-term velocity trends. Our sample of stars contains eight known companions with mass ($M_p \sin i$) less than 8 Jupiter masses (M_J), six of which were discovered at Lick. For the remaining stars, we place upper limits on the companion mass as a function of orbital period. For most stars, we can exclude companions with velocity amplitude $K \gtrsim 20$ m s^{-1} at the 99% level, or $M_p \sin i \gtrsim 0.7 M_J (a/\mathrm{AU})^{1/2}$ for orbital radii $a \lesssim 5$ AU. We examine the implications of our results for the observed distribution of mass and orbital radius of companions. We show that the combination of intrinsic stellar variability and measurement errors most likely explains why all confirmed companions so far have $K \gtrsim 40$ m s^{-1}. The finite duration of the observations limits detection of Jupiter-mass companions to $a \lesssim 3$ AU. Thus it remains possible that the majority of solar-type stars harbor Jupiter-mass companions much like our own, and if so these companions should be detectable in a few years. It is striking that more massive companions with $M_p \sin i > 3 M_J$ are rare at orbital radii 4–6 AU; we could have detected such objects in $\sim$90% of stars, yet found none. The observed companions show a "piling-up" toward small orbital radii, and there is a paucity of confirmed and candidate companions with orbital radii between $\sim$0.2 and $\sim$1 AU. The small number of confirmed companions means that we are not able to rule out selection effects as the cause of these features. We show that the traditional method for detecting periodicities, the Lomb-Scargle periodogram, fails to account for statistical fluctuations in the mean of a sampled sinusoid, making it nonrobust when the number of observations is small, the sampling is uneven, or for periods comparable to or greater than the duration of the observations. We adopt a "floating-mean" periodogram, in which the zero point of the sinusoid is allowed to vary during the fit. We discuss in detail the normalization of the periodogram and the probability distribution of periodogram powers. We stress that the three different prescriptions in the literature for normalizing the periodogram are statistically equivalent and that it is not possible to write a simple analytic form for the false alarm probability, making Monte Carlo methods essential.

Subject headings: binaries: spectroscopic — methods: statistical — planetary systems

1. INTRODUCTION

In the past few years, high-precision radial velocity surveys have had remarkable success in the discovery of planetary-mass companions around nearby solar-type stars (for reviews, see Marcy & Butler 1998 and Marcy, Cochran, & Mayor 1999). Searches for companions (Campbell, Walker, & Yang 1988; McMillan et al. 1994; Mayor & Queloz 1995; Walker et al. 1995; Cochran et al. 1997; Noyes et al. 1997; Marcy & Butler 1992, 1998) have been carried out with Doppler velocity precision $\approx$10 m s^{-1}, although 3 m s^{-1} has been achieved at Lick observatory for chromospherically quiet stars (Butler et al. 1996). There are now 17 companions known with masses (the observable is $M_p \sin i$, where i is the angle of inclination of the orbit with respect to the line of sight) below 10 Jupiter masses. In total, several hundred stars have been monitored for timescales of 3 yr to more than 11 yr. The detections so far suggest that a few percent of solar-type stars harbor companions of a Jupiter mass or more within a few AU.

These objects have raised many questions regarding the distribution of the mass and orbital radius of planetary-mass companions and the relation of these systems to our own solar system and its giant planets. For example, a surprise was the discovery of Jupiter-mass companions in close proximity to their host star. Of the 17 companions within 2.5 AU, 13 have semimajor axis $a < 0.5$ AU, and five have $a < 0.1$ AU. The archetypal example is the companion orbiting 51 Pegasi (Mayor & Queloz 1995), which has a mass ($M_p \sin i$) of 0.44 Jupiter masses (M_J) and an orbital radius $a = 0.05$ AU, 8 times closer than Mercury's orbit about the Sun. The orbital parameters of the 17 planetary-mass companions are listed in Table 1.

Unfortunately, gleaning the true distribution of companions is complicated by selection effects that favor the detection of massive, close companions. It is necessary to establish detection thresholds for searches for planetary-mass companions before the observations can be fully interpreted. Walker et al. (1995) monitored 21 bright solar-type stars for 12 yr. They carried out a detailed statistical analysis and from their upper limits could exclude companions with $M_p \sin i \sim 1$–$3\ M_J$ for periods less than the duration of their observations ($\approx$12 yr). Nelson & Angel (1998) used a simple analytic formalism, together with comparisons with real data, to investigate the dependence of detection thresholds on the number and duration of observations and the Doppler errors.

Our aim in this paper is to place the confirmed companions from the Lick radial velocity survey in context by an analysis of the null detections. The ongoing Lick survey consists of more than 11 yr of precision Doppler velocity

[1] Department of Physics, 366 LeConte Hall, University of California, Berkeley, CA 94720; cumming@fire.berkeley.edu.
[2] Department of Astronomy, 601 Campbell Hall, University of California, Berkeley, CA 94720.
[3] Department of Physics and Astronomy, San Francisco State University, San Francisco, CA 94132; gmarcy@stars.sfsu.edu.
[4] Anglo-Australian Observatory, PO Box 296, NSW 1710 Epping, Australia; paul@aaoepp.aao.gov.au.

TABLE 1

ORBITS OF KNOWN PLANETARY-MASS COMPANIONS

Star Name	Lick Survey?[a]	Spectral Type	P (days)	a (AU)	K (m s^{-1})	$M_p \sin i$	e (M_J)	References
HD 187123		G3 V	3.10	0.042	83	0.57	0.03	1
τ Boo (HR 5185)	Y	F7 V	3.31	0.047	468	3.66	0.00	2
51 Peg (HR 8729)		G5 V	4.23	0.051	56	0.44	0.01	3, 4
υ And (HR 458)	Y	F8 V	4.62	0.054	71.9	0.61	0.15	2
HD 217107		G7 V	7.12	0.072	140	1.28	0.14	5
ρ^1 55 Cnc (HR 3522)	Y	G8 V	14.7	0.11	75.9	0.85	0.04	2
Gliese 86		K1 V	15.8	0.114	379	4.9	0.04	6
HD 195019		G3 V/IV	18.3	0.136	275	3.43	0.03	5
ρ CrB (HR 5968)		G2 V	39.6	0.23	67	1.1	0.11	7
Gliese 876	Y	M4	61	0.21	217	2.1	0.27	8, 9
HD 168443		G8 IV	57.9	0.28	350	4.96	0.54	10
HD 114762		F7 V	84.0	0.41	618	11.0	0.33	10, 11
70 Vir (HR 5072)	Y	G2.5 V	117	0.47	316	7.4	0.40	12
HD 210277		G7 V	437	1.20	42	1.28	0.45	10
16 Cyg B (HR 7504)	Y	G2.5	799	1.6	50.3	1.67	0.69	13
47 UMa (HR 4277)	Y	G0 V	1092	2.1	47	2.38	0.11	14
14 Her		K0 V	1620	2.5	75	3.3	0.36	15

[a] We indicate with a "Y" those companions discovered by the original Lick survey.

REFERENCES.—(1) Butler et al. 1998; (2) Butler et al. 1997; (3) Mayor & Queloz 1995; (4) Marcy et al. 1997; (5) Fischer et al. 1999; (6) Queloz et al. 1999; (7) Noyes et al. 1997; (8) Marcy et al. 1998; (9) Delfosse et al. 1998; (10) Marcy et al. 1999; (11) Latham et al. 1989; (12) Marcy & Butler 1996; (13) Cochran et al. 1997; (14) Butler & Marcy 1996; (15) Mayor et al. 1998.

measurements of 107 stars (a few of which have been added or dropped as the survey progressed), and 200 new stars have recently been added (Fischer et al. 1999). The original program has so far identified six planetary-mass companions (70 Vir, 47 UMa, 55ρ Cnc, τ Boo, υ And, and Gl 876; they are marked in Table 1), codiscovered the companion to 16 Cyg B, and confirmed two discoveries made by other groups (51 Peg and ρ CrB; see Table 1 for orbital parameters and references).

We search for periodicities and place upper limits using the "floating-mean periodogram," an extension of the well-known Lomb-Scargle periodogram (Lomb 1976; Scargle 1982) in which we fit sinusoids to the data but allow the zero point of the sinusoid to "float" during the fit. This approach was adopted by Walker et al. (1995), who were interested in obtaining correct upper limits for periods greater than the duration of the observations. We show here that allowing the mean to float is crucial to account for statistical fluctuations in the mean of a sampled sinusoid. The traditional Lomb-Scargle periodogram fails in precisely the regime in which we demand it be robust, namely when the number of observations is small, the sampling is uneven, or the period of the sinusoid is comparable to or greater than the duration of the observations. We carefully consider the correct normalization of the periodogram, an issue that has been of some debate in the literature (Horne & Baliunas 1986; Gilliland & Baliunas 1987; Schwarzenberg-Czerny 1996).

The plan of the paper is as follows. We begin in § 2 by describing the observations and estimating the velocity variability we expect to see due to measurement error and intrinsic stellar effects. We discuss in § 3 our methods for searching for the signatures of companions in the radial velocity data. We look for variability in excess of our prediction, long-term trends, and periodicities. We list those stars for which we see interesting variability or periodicities that may indicate the presence of a yet unconfirmed companion. In § 4, we place upper limits on the mass of a possible companion as a function of orbital radius for each star in the sample. We continue in § 5 with a discussion of the implications of our results for the occurrence rate of planetary-mass companions to solar-type stars and their distribution in mass and orbital radius. We present our conclusions in § 6. In Appendix A, we give a brief derivation of the periodogram, and in Appendix B, we discuss its normalization.

2. OBSERVATIONS

The Lick radial velocity survey is now more than 11 yr old (Marcy & Butler 1992, 1998). Precise radial velocity measurements (current precision ~ 5 m s^{-1}; Butler et al. 1996) are made with the Lick 3 m telescope by using an echelle spectrograph and a comparison iodine reference spectrum. The exposure time is 10 minutes for a star with $V = 5$, allowing several observations per year for each star in the sample. In this paper, we present an analysis of observations of 76 F-, G-, and K-type stars in the original survey.[5] A summary of the observations is given in Table 2. For each star, we give its HR and HD catalog number, spectral type, and rotation period. We list the number and duration of the observations, the typical internal velocity error, and the rms scatter of the data. Radial velocities are available upon request from G. Marcy.

2.1. *Distribution of Errors and Intrinsic Stellar Variability*

Two sources of variability can mask velocity variations due to a companion: measurement uncertainties and intrinsic stellar variability. In this section, we attempt to quantify these effects.

[5] There have been observations of 29 M dwarfs as part of the survey, but we do not include these in our analysis as they are faint ($V > 7$) and suffer from large measurement uncertainties. These stars are part of a sample being monitored with the Keck telescope. An analysis of their radial velocity variability will be presented elsewhere.

TABLE 2

SUMMARY OF THE OBSERVATIONS

STAR		SPECTRAL	P_{rot} [a]	$\langle\sigma_D\rangle$ [b]	σ_{rms}		T
HR	HD	TYPE	(days)	(m s^{-1})	(m s^{-1})	N	(yr)
8	166	K0	5.7	20/7.4	18.5	41	11.4
88	1835	G3	8	26/15	40.8	56	11.2
166	3651	K0	44	15/7.1	12.2	70	11.2
219a	4614	G0	15	23/6.2	40.5	69	11.1
222	4628	K2	39	18/7.0	14.4	40	11.2
458	9826	F8	12	29/14	74.2	110	11.2
493	10476	K1	35	16/6.0	8.93	38	10.3
509	10700	G8	34	18/6.6	10.3	278	11.2
582	12235	G2	14	23/8.8	15.4	34	10.4
753	16160	K3	48	17/6.9	38.7	33	10.4
799	16895	F8	7	26/13	15.5	43	11.2
857	17925	K2	6.9	18/9.4	25.4	27	11.2
937	19373	G0	21	18/6.5	11.5	131	11.2
962	19994	F8	10	24/14	30.1	29	11.2
996	20630	G5	9	22/7.5	24.4	67	11.2
1084	22049	K2	12	19/5.9	19.2	121	11.2
1101	22484	F9	18	19/6.8	15.2	40	11.2
1262	25680	G5	9	22/7.7	20.7	30	11.2
1325	26965	K1	43	22/6.6	22.4	66	11.2
1614	32147	K3	47	17/5.8	7.67	30	11.2
1729	34411	G2	24	17/7.8	9.43	106	11.2
1925	37394	K1	11	19/6.7	19.1	12	4.91
2047	39587	G0	5.2	43/13	1430	36	11.2
2483	48682	G0	14	22/11	13.6	61	11.2
2643	52711	G4	19	26/8.3	19.9	36	11.2
3262	69897	F6	2.9	32/13	22.4	56	11.2
3522	75732	G8	44	16/7.9	60.7	114	8.91
3538	76151	G3	15	24/8.4	16	32	8.81
3625	78366	F9	10	26/11	24.2	28	9
3881	84737	G0	23	18/8.4	12.1	62	10.9
3951	86728	G2	27	17/7.9	11.4	75	10.5
4112	90839	F8	7.3	32/7.2	19.7	35	8.28
4277	95128	G0	16	22/7.5	31.1	86	11.4
4345	97334	G0	8	25/16	30.4	36	10.5
4496	101501	G8	17	21/8.7	14.9	72	11
4540	102870	F9	14	25/6.8	17.5	80	10.5
4983	114710	G0	12	24/7.0	27	100	9.71
5011	115383	G0	3.5	29/13	26.5	40	8.89
5019	115617	G6	29	20/6.9	15.4	46	7.21
5072	117176	G2	36	19/7.4	185	92	10.4
5185	120136	F7	4	61/24	331	80	11.1
5273	122742	G8	30	25/8.6	4300	24	9.71
5384	126053	G1	22	24/9.0	15.1	29	10.1
5447	128167	F2	0.3	53/24	51.8	48	10.3
5534	130948	G0	3.2	29/14	33.4	24	10.1
5544a	131156	G8	6	23/8.1	67	60	11.0
5544b	131156b	K4	11	21/13	91.3	23	10.1
5553	131511	K2	10	18/11	8880	20	7.85
5568	131977	K4	40	18/9.7	11.3	47	5.06
5868	141004	G0	26	18/7.0	10.8	106	10.9
5914	142373	F8	15	26/8.8	15.9	83	10.8
5933	142860	F6	3	56/19	64.9	70	9.15
5968	143761	G2	30	…/8.5	31	20	1.21
6171	149661	K2	21	17/7.8	11.2	40	7.31
6458	157214	G0	22	21/9.6	14.3	72	11.2
6623	161797	G5	42	13/5.4	146	76	11
6806	166620	K2	43	17/7.4	14.9	39	11.1
6869	168723	K2	44	14/5.4	15	47	11
7061	173667	F6	2.3	64/36	129	78	11.2
7462	185144	K0	27	16/6.4	12.2	42	9.3
7503	186408	G1	27	19/10	18.8	62	11.4
7504	186427	G2	29	21/11	29.4	124	11.4

TABLE 2—*Continued*

Star		Spectral	P_{rot} [a]	$\langle\sigma_D\rangle$ [b]	σ_{rms}		T
HR	HD	Type	(days)	(m s^{-1})	(m s^{-1})	N	(yr)
7602	188512	G8	52	15/5.7	13.2	85	11.4
7672	190406	G1	14	21/9.7	87.7	74	11
8085	201091	K5	35	17/6.0	10.6	100	11.4
8086	201092	K7	38	18/7.2	31.9	58	11.4
8314	206860	G0	5	37/19	33.8	36	9.89
8382	208801	K2	45	17/6.1	7.77	21	5.29
8665	215648	F6	3.6	30/16	26.9	61	11
8729	217014	G5	22	.../11	40.5	220	2.77
8832	219134	K3	48	16/7.6	13.4	45	5.86
8969	222368	F7	9	26/10	23.7	60	9.89
Gl 250a	50281	K3	45	17/7.6	15.1	18	5.01
Gl 641	152391	G6	11	13/11	24	29	5.18
Gl 688	160346	K3	37	11/7.1	3730	7	3.99
Gl 716	170657	K3	15	8.6/16	15.8	13	4.87

[a] Rotation periods are from Baliunas et al. 1996, Soderblom 1985, or D. A. Fischer 1999 (private communication).

[b] We give the mean internal Doppler error before and after 1994 November. The internal errors have been augmented as described in § 2.1.

The uncertainty in the radial velocity measurement v is estimated for each observation from the dispersion of the velocities measured by different spectral segments of the spectrometer. An upgrade to the spectrograph optics and improvements in modeling in 1994 November led to an increase in the Doppler precision from $\sigma_D \sim 10$–15 m s^{-1} to $\sigma_D \sim 5$ m s^{-1}, with $\sigma_D \sim 3$ m s^{-1} achievable in the best cases. This improved Doppler precision is dominated by photon statistics (for a detailed discussion, see Butler et al. 1996). In this paper, we shall refer to the pre–1994 November data as "pre-fix" and post–1994 November data as "post-fix." Table 2 gives the average internal error $\langle\sigma_D\rangle$ before and after 1994 November for each star.

Intrinsic stellar variability arises from magnetic activity or rotation of features across the stellar surface, such as sunspots or inhomogeneous convective patterns (Saar & Donahue 1997). Saar, Butler, & Marcy (1998, hereafter SBM98) used the Lick radial velocity variations (post-fix data only) to characterize the relationship between the rotation period, P_{rot}, of a star and its intrinsic velocity variability, σ_V. They found that the variability in excess of the internal errors could be explained by simple models of sunspot rotation and inhomogeneous convective flows. We use their results to estimate the typical intrinsic variability associated with such effects as a function of stellar rotation period.[6] After inspecting Figure 2 of SBM98, we find $\sigma_V = 10 \text{ m s}^{-1}(12 \text{ days}/P_{rot})^{1.1}$ for G- and K-type stars and $\sigma_V = 10 \text{ m s}^{-1}(10 \text{ days}/P_{rot})^{1.3}$ for F stars. The rotation period for each star (taken from Soderblom 1985, Baliunas, Sokoloff, & Soon 1996, or D. Fischer 1999, private communication) is given in Table 2.

We obtain the total estimated variability for each data point by adding the intrinsic variability to the internal error in quadrature, $\sigma_j^2 = \sigma_V^2 + \sigma_{D,j}^2$ (here we label each data point with the index j). How well does this estimate reproduce the scatter in the data? After a preliminary analysis of the post-fix data (using the methods of §§ 3.1 and 3.2), we selected a subset of 26 stars that had no excess variability or long term trends. In Figure 1, we plot a histogram (*solid line*) of individual radial velocity measurements v_j divided by the estimated variability σ_j for this subset of stars. For each star, we have subtracted the weighted mean of the velocities. The upper panel shows the pre-fix data; the lower panel shows the post-fix data. The dotted histogram in each case shows a Gaussian distribution with unit variance. If the scatter in the velocities were Gaussian with variance σ_j^2 for each point, the dotted and solid histograms would match. They do not, indicating more scatter in the data than we expect. In addition, the pre-fix and post-fix v/σ distributions are different.

The excess scatter may be due to a combination of underestimated internal errors and systematic errors in the velocities, particularly for the early observations. We have chosen to augment the internal errors by multiplying by a constant factor to force the observed v/σ distribution to match a Gaussian with unit variance. In this way, *we bring the pre-fix and post-fix v/σ distributions into agreement*, and we are confident that we have not underestimated the errors. For all 76 stars in our sample, we multiply the pre-fix internal errors by 1.7 and the post-fix internal errors by 1.4. The dashed histograms in Figure 1 show the v/σ distributions using these rescaled internal errors. The distribution is unchanged if we remove the 10 chromospherically active stars in this subset which have $P_{rot} \leq 12$ days. *Hereafter, we refer to the augmented internal errors as simply* "internal errors."

In Figure 2, we show the effect of including the intrinsic variability prediction σ_V for stars of different rotation period. For each star in the subset of 26 stars of Figure 1, we plot $\chi_v^2 = \sum (v_j/\sigma_j)^2/(N-1)$ as a function of P_{rot}. We show χ_v^2 evaluated using the internal errors only (*crosses*) and including the intrinsic variability added in quadrature (*squares*). The extra variability of stars with short rotation periods ($P_{rot} \lesssim 12$ days) is shown by the large uncorrected χ^2 values for these stars. The mean value of χ_v^2 in Figure 2 is less than unity, indicating that our procedure may have overestimated the internal errors somewhat. However, we prefer to err on the side of *over*estimation.

[6] At first sight, it may seem circular to use the work of SBM98, which was based on the Lick data set (the post-fix data only). However, our approach is to use their results to characterize the *average* variability typical for a star in the survey with a particular rotation period.

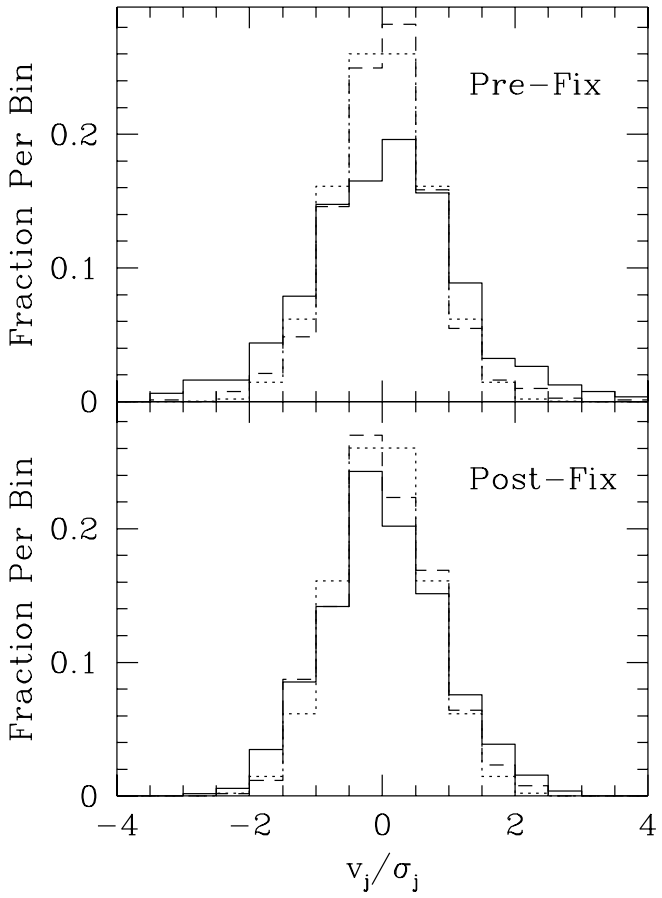

FIG. 1.—Distribution of Doppler velocities v_j in the pre-fix and post-fix data. A histogram of the velocities v_j divided by the estimated error σ_j is shown (*solid line*) for a subset of 26 stars. These stars, selected from a preliminary analysis of the *post-fix* data, have no significant trend or excess variability. The number of pre-fix (post-fix) observations is 801 (515). The dotted line in each panel shows a Gaussian distribution with unit variance. The dashed line in the upper (lower) panel shows the effect of increasing the pre-fix (post-fix) internal errors by a constant factor of 1.7 (1.4). These increased internal errors are the ones we adopt for all stars in our analysis.

We use the variability estimate σ_j in two ways. The first is to identify those stars that show much more variability than we might expect given their rotation periods (§ 3.2). The second is to weight the data points when we look for periodicities (§ 3.4). The large difference between the pre-fix and post-fix data makes it important to give less weight to the early data points. Not only are the pre-fix errors larger, they are less well characterized than the post-fix errors. One might question the value of including the low-quality early data points at all. However, they are important because they extend the time baseline, allowing us to search for longer period companions.

3. SEARCH FOR COMPANIONS

The velocity amplitude K of a star of mass M_* due to a companion with mass $M_p \sin i$ with orbital period P and eccentricity e is

$$K = \left(\frac{2\pi G}{P}\right)^{1/3} \frac{M_p \sin i}{(M_p + M_*)^{2/3}} \frac{1}{\sqrt{1-e^2}} . \quad (1)$$

For a circular orbit with $M_p \ll M_*$, the velocity variations

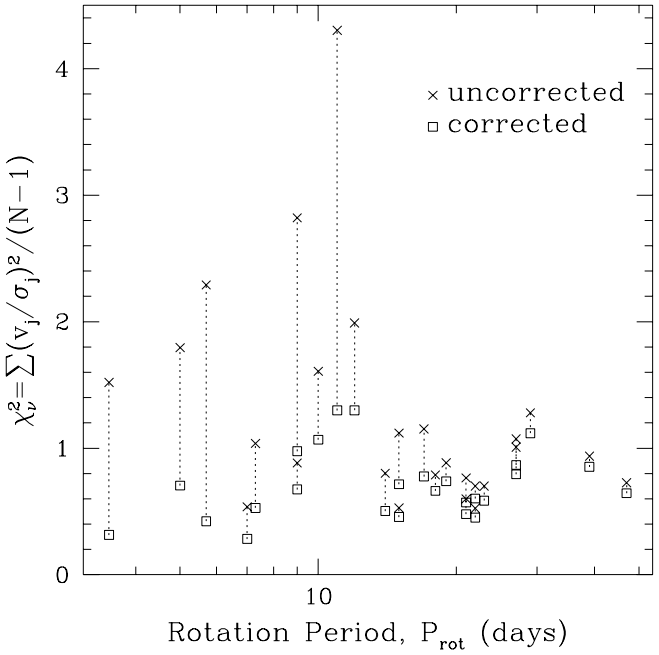

FIG. 2.—Weighted sum of squares of velocity, $\chi^2 = \sum (v_j/\sigma_j)^2/(N-1)$, as a function of rotation period for the 26 stars of Fig. 1. We show the sum evaluated using internal errors only (*crosses*) and internal errors plus estimated intrinsic variability (*squares*). The intrinsic variability in stars with $P_{rot} \lesssim 14$ days is shown by the large uncorrected χ^2 values for these stars.

are sinusoidal with amplitude

$$K = 28.4 \text{ m s}^{-1} \left(\frac{1 \text{ yr}}{P}\right)^{1/3} \left(\frac{M_p \sin i}{M_J}\right) \left(\frac{M_\odot}{M_*}\right)^{2/3} , \quad (2)$$

where M_J is the mass of Jupiter. The orbital period is related to the orbital radius by Kepler's law,

$$P = 1 \text{ yr } (a/\text{AU})^{3/2} (M_\odot/M_*)^{1/2} . \quad (3)$$

For example, the companion to 51 Peg ($a = 0.05$ AU, $M_p \sin i = 0.44$) induces a velocity amplitude $K = 56$ m s^{-1}, whereas Jupiter ($a = 5.2$ AU, $P = 11.9$ yr) gives $K = 12.5$ m s^{-1} for the Sun.

In this section, we describe the methods we use to search for such a signal and present our results. For each star in Table 2, we first ask if there is a significant long-term trend in the data, and if so we subtract it (§ 3.1). We then ask if the observed scatter in the data is consistent with the expected variability (§ 3.2). To search for periodicities (§ 3.4), we fit sinusoids to the data, employing a generalization of the well-known Lomb-Scargle periodogram (§ 3.3). By using sinusoids as our basic model for the data, we are strictly assuming circular orbits, although we find that the periodogram gives a good estimate of the orbital period even for eccentric orbits. This is because, to lowest order in the eccentricity, the radial velocity signal from an eccentric orbit has its main component at the orbital frequency (with smaller components at multiples of the orbital frequency). We discuss a possible extension of the periodogram to Kepler orbits in the conclusions (§ 6). The normalization of the periodogram has been of some question in the literature, so we discuss our choice of normalization in Appendix B. We close this section by summarizing our results and indicating those stars that show interesting variability or evidence for companions (§ 3.5).

3.1. *Long-Term Trends*

We first ask if there is a significant *long-term* trend, on a

timescale much greater than the duration of the observations (i.e., $\gg 10$ yr). For each star, we fit a straight line $v_j = at_j + b$ to the measured velocities. When calculating χ^2 for the fit, we weight each point by the inverse square of the estimated error, $w_j = 1/\sigma_j^2$. We give the best-fit slope and its uncertainty (as derived from the least-squares fit) in Table 3.

To assess the significance of each slope, we ask if the coefficient of the linear term is significantly nonzero. We use the F-test to compare the weighted sum of squares of residuals from the straight line fit χ^2_{N-2} (two free parameters) to the weighted sum of squares about the mean χ^2_{N-1} (one free parameter). If there is no long-term trend and the residuals are Gaussian distributed, the statistic

$$F = (N-2)\,\frac{\chi^2_{N-1} - \chi^2_{N-2}}{\chi^2_{N-2}} \qquad (4)$$

follows Fisher's F distribution (Bevington & Robinson 1992) with 1 and $N-2$ degrees of freedom. Given the distribution $F_{1,N-2}$, we calculate the probability that F would exceed the observed value $F_{\rm obs}$ purely by chance (the false alarm probability). We give the F-test false alarm probabilities for each star in Table 3.

The slopes listed in Table 3 contain much information about possible companions at long periods. For the purposes of this paper, however, we are interested in identifying slopes that would directly affect our search for companions with $P \lesssim 30$ yr. Thus, we mark with $*$ in Table 3 those stars that have a slope ≥ 5 m s^{-1} yr^{-1} and an F-test false alarm probability less than 10^{-5}. We adopt a higher threshold (10^{-5}) than elsewhere in this paper because systematic effects in the pre-fix data or variations due to magnetic activity on long timescales can imitate a slope. The stars marked with $*$ in Table 3 are HR 219a, HR 753, HR 1325, HR 2047, HR 5544a, HR 5544b, HR 6623, HR 7672, and HR 8086.[7]

3.2. *Excess Variability*

We now ask if the scatter in the velocities is consistent with our predicted variability for each star (§ 2.1). The χ^2 about the mean, χ^2_{N-1}, or (for those stars marked $*$ in Table 3) about the best-fit straight line, χ^2_{N-2}, gives us a measure of variability. We use the χ^2 distribution with $N-m$ degrees of freedom to test if the velocities are consistent with being drawn from a Gaussian distribution with variance σ_j^2. Here m is the number of parameters in the model of the data, $m = 2$ for a straight line or $m = 1$ for a mean. A small false alarm probability indicates there is more variability in the data than we expect. The results of this test are shown in Table 4. We indicate with a $*$ those stars that have false alarm probabilities less than 1%. We choose a 99% threshold so that there will be no more than one false signal in our sample of 76 stars. The stars that show significant variability are HR 88, HR 166, HR 2047, HR 4345, HR 5273, HR 5544b, HR 5553, HR 7061, Gl 641, Gl 688, and the stars with confirmed planetary-mass companions (listed in Table 1).

3.3. *The Floating-Mean Periodogram*

In this section, we test for periodicity in the data using what we refer to as the "floating-mean periodogram," a

[7] HR 8085, the companion to HR 8086, would have exhibited a slope had we removed the effect of secular acceleration; see § 3.5.

TABLE 3

TEST FOR LONG-TERM TRENDS (F-TEST)[a]

Star (HR)	Slope (m s^{-1} yr^{-1})	N	$F_{1,N-2}$	False Alarm
8	-1.5 ± 1.7	41	1.8	0.187
88	-1.1 ± 1.4	56	0.206	0.652
166	0.68 ± 0.58	70	0.835	0.364
*219a	9.3 ± 0.58	69	681	8.13E−37
222	0.76 ± 0.72	40	1.31	0.259
458	-6.6 ± 0.82	110	3.47	0.0651
493	1.4 ± 0.68	38	9.36	0.00418
509	0.82 ± 0.29	278	16.3	7.1E−05
582	-3.9 ± 1.3	34	28.5	7.33E−06
*753	12 ± 0.73	33	399	2.95E−19
799	-1.6 ± 1.4	43	4.77	0.0348
857	3.5 ± 2.2	27	2.09	0.161
937	1.2 ± 0.39	131	20.4	1.4E−05
962	3.3 ± 1.2	29	4.35	0.0466
996	-3.1 ± 0.89	67	9.56	0.0029
1084	1.4 ± 0.44	121	10.4	0.00161
1101	0.2 ± 0.71	40	0.118	0.734
1262	0.015 ± 1.4	30	0.000103	0.992
*1325	5 ± 0.45	66	152	1.49E−18
1614	1.7 ± 0.89	30	6.42	0.0172
1729	1.6 ± 0.39	106	29.8	3.3E−07
1925	-4.6 ± 2.8	12	2.38	0.154
*2047	310 ± 1.8	36	232	9.5E−17
2483	-0.31 ± 0.77	61	0.317	0.576
2643	2.2 ± 1.2	36	5.12	0.0301
3262	1.9 ± 1.1	56	3.83	0.0557
3522	-3.7 ± 0.67	114	0.442	0.508
3538	1.2 ± 1.5	32	0.991	0.327
3625	0.79 ± 1.9	28	0.153	0.699
3881	0.2 ± 0.57	62	0.205	0.652
3951	1.8 ± 0.63	75	10.4	0.00185
4112	-2.9 ± 1.5	35	8.75	0.00569
4277	2.2 ± 0.69	86	2.19	0.142
4345	1.7 ± 1.9	36	0.447	0.508
4496	1.3 ± 0.58	72	6.69	0.0118
4540	1.3 ± 0.62	80	3.93	0.051
4983	3.2 ± 0.68	100	20.3	1.83E−05
5011	-1.8 ± 3.3	40	0.893	0.351
5019	4.4 ± 0.88	46	43.8	4.13E−08
5072	-3.1 ± 0.55	92	0.073	0.788
5185	-23 ± 1.8	80	3.43	0.0677
5273	850 ± 1.5	24	13.5	0.00132
5384	-1.3 ± 1.1	29	3.09	0.0902
5447	-2.2 ± 1.8	48	1.21	0.277
5534	-3.5 ± 1.7	24	1.61	0.217
*5544a	18 ± 1.1	60	197	2.8E−20
*5544b	-25 ± 1.2	23	187	6.27E−12
5553	1000 ± 1.3	20	2.46	0.134
5568	-3.6 ± 1.3	47	7.32	0.00959
5868	-0.98 ± 0.49	106	4.27	0.0413
5914	1.5 ± 0.64	83	13.5	0.000422
5933	-8.1 ± 1.6	70	20.2	2.78E−05
5968	-19 ± 5.5	20	0.957	0.341
6171	-0.56 ± 1.1	40	0.586	0.449
6458	1.8 ± 0.58	72	20.2	2.71E−05
*6623	-47 ± 0.41	76	11800	2.05E−83
6806	1.3 ± 0.68	39	3.3	0.0775
6869	0.19 ± 0.69	47	0.0464	0.83
7061	-8.2 ± 2	78	3.07	0.0836
7462	0.86 ± 0.6	42	2.63	0.113
7503	-3 ± 0.7	62	18.2	7.05E−05
7504	-1.9 ± 0.69	124	1.29	0.258
7602	2 ± 0.42	85	25	3.21E−06
*7672	-24 ± 0.6	74	2310	1.92E−56

TABLE 3—*Continued*

Star (HR)	Slope (m s^{-1} yr^{-1})	N	$F_{1,N-2}$	False Alarm
8085	0.59±0.4	100	4.5	0.0364
*8086	8.9±0.59	58	326	4.96E−25
8314	−6.8±2.9	36	9.95	0.00335
8382	1.5±1.4	21	1.99	0.174
8665	−3.7±1.2	61	11.7	0.00112
8729	−2.3±1.8	220	0.106	0.745
8832	2.8±1.1	45	9.02	0.00444
8969	−1±1.1	60	1.2	0.277
Gl 250a.....	−0.53±1.5	18	0.0803	0.781
Gl 641	0.35±2.1	29	0.00937	0.924
Gl 688	−2200±2.5	7	6.5	0.0514
Gl 716	0.38±2.2	13	0.0353	0.854

[a] We mark with "*" in the leftmost column those stars for which we subtract the slope from the data (§ 3.1). These stars have a false alarm probability less than 10^{-5} and a slope greater than 5 m s^{-1} yr^{-1}.

generalization of the well-known Lomb-Scargle periodogram (Lomb 1976; Scargle 1982). We define the floating-mean periodogram as follows. For each trial frequency $\omega = 2\pi/P$, we start with a simple model for the data, namely a sinusoid plus a constant term,

$$f_j = A \cos \omega t_j + B \sin \omega t_j + C \,, \tag{5}$$

where t_j are the observation times. We perform a linear least-squares fit of this model to the data, to determine the constants A, B, and C. The periodogram is an "inverted" plot of the χ^2 of this fit as a function of frequency. We define the floating-mean periodogram power $z(\omega)$ as

$$z(\omega) = \frac{(N-3)}{2} \frac{\chi^2_{N-1} - \chi^2(\omega)}{\chi^2(\omega_0)} \,, \tag{6}$$

where $\chi^2(\omega) = \sum w_j[v_j - f_j(\omega)]^2$ is the χ^2 of the fit, ω_0 is the best-fit frequency (i.e., the frequency that gives the maximum periodogram power), and χ^2_{N-1} is the weighted sum of squares about the mean. When calculating χ^2, we weight each data point by $w_j \propto 1/\sigma_j^2$ as in § 3.1. We use a linear least-squares fitting algorithm from Press et al. (1992) to fit equation (5) to the data and find $\chi^2(\omega)$. The choice of normalization of the periodogram has been a subject of some debate in the literature; we discuss this in detail in Appendix B. We normalize by the weighted sum of squares of the residuals to the best-fit sinusoid, $\chi^2(\omega_0)$.

The Lomb-Scargle periodogram is obtained by considering a fit of a sinusoid only, i.e., the case $C \equiv 0$ in equation (5) (we sketch the derivation of the Lomb-Scargle formula from the least-squares approach in Appendix A). This means that the zero point of the sinusoid is assumed to be known already. In practice, the mean of the data is taken as an estimate of the zero point and is subtracted from the data before applying the Lomb-Scargle formula. In our approach, the zero point of the sinusoid is an additional free parameter at each frequency, i.e., the mean of the data is allowed to "float" during the fit.

This approach has been adopted by other authors. Ferraz-Mello (1981) was the first to do so, defining the "date-compensated discrete Fourier transform." Walker et al. (1995) generalized to the case where a straight line or quadratic function was subtracted from the data, defining a "correlated periodogram." Most recently, Nelson & Angel (1998) included a constant term in their Monte Carlo experiments. These authors were concerned about the suppression of periodogram power for periods greater than the duration of the observations. We show here that allowing the mean to float is important under much more general circumstances.

We now provide some examples that show that allowing the mean to float is crucial if the number of observations is small, the sampling is uneven, or there is a period comparable to the duration of the observations or longer. Figure 3 shows simulated data of a companion in a circular orbit with $P = 9.6$ yr and $K = 15$ m s^{-1} ($a = 4.5$ AU, $M_p \sin i = 1.1\ M_J$). We use the observation times and errors for one of the stars in our sample, HR 222. The upper panel shows the velocity measurements as a function of time. The dashed line shows the mean of the data, which is about 10 m s^{-1} greater than the correct zero point of the sine wave. The solid line shows the best-fit sinusoid when the mean is allowed to float. The traditional and floating-mean periodograms are shown in the lower panel. The power at long periods is significantly less in the traditional periodogram than the floating mean periodogram. Black & Scargle (1982) first noted this effect in their analysis of astrometric data, where they showed that proper motions could significantly reduce the measured amplitude of long period signals (see Fig. 3 of Black & Scargle 1982).

The upper panel in Figure 4 shows 20 velocities obtained at Lick for the star HR 5968, which has a known companion with $K = 67$ m s^{-1} and $P = 39.6$ days (Noyes et al.

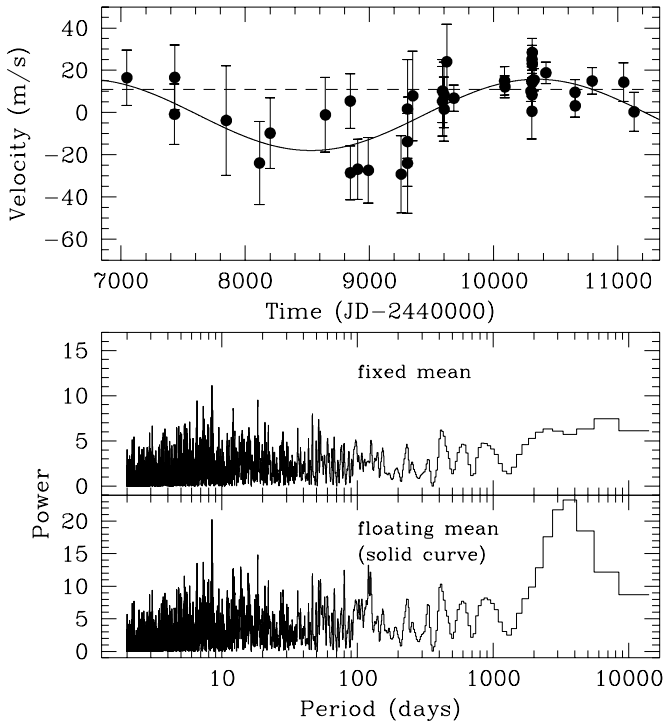

FIG. 3.—Example of the difference between fitting a sinusoid with the mean of the data subtracted in advance, and fitting a sinusoid with the mean allowed to "float" as an extra free parameter. The upper panel shows simulated data of a sinusoid with $P = 9.6$ yr and amplitude $K = 15$ m s^{-1}. We use the observation times and Doppler errors for HR 222. The floating-mean periodogram (*lower panel*) obtains the correct period ($P = 3637$ days), and the rms of the residuals is 7.7 m s^{-1}. The traditional periodogram has a maximum at $P = 8.5$ days. The subtraction of the mean results in a suppression of power at long periods. To allow for a fair comparison, the vertical scales have a ratio of the square of the rms to account for the different normalization factors.

TABLE 4

TEST FOR EXCESS VARIABILITY (χ^2-TEST)[a]

Star (HR)	Expected rms[b] (m s^{-1})	Observed rms[c] (m s^{-1})	χ^2_ν	False Alarm
8	28.5	18.5	0.423	0.999
*88	25.3	40.8	2.78	3.94E−11
*166	10.2	12.2	1.64	0.000676
219a	21.1	18.6	0.379	1
222	14	14.4	0.853	0.728
*c 458	21	74.2	19.3	0
493	12.6	8.93	0.551	0.988
509	14.2	10.3	0.512	1
582	19.3	15.4	0.591	0.97
753	13.3	10.7	0.622	0.95
799	26.7	15.5	0.283	1
857	24	25.4	1.33	0.118
937	16.8	11.5	0.571	1
962	23.9	30.1	1.59	0.024
996	23.2	24.4	1.43	0.0122
1084	19.9	19.2	1.07	0.29
1101	17.6	15.2	0.662	0.948
1262	20.9	20.7	0.976	0.502
1325	17.9	19	0.795	0.883
1614	11.1	7.67	0.645	0.929
1729	13	9.43	0.712	0.989
1925	17.8	19.1	1.3	0.217
*2047	42.7	364	125	0
2483	19.1	13.6	0.504	1
2643	20.1	19.9	0.738	0.87
3262	56.5	22.4	0.14	1
*c 3522	9.81	60.7	70.1	0
3538	19.2	16	0.716	0.877
3625	22.4	24.2	1.07	0.369
3881	15.7	12.1	0.585	0.996
3951	12.4	11.4	0.868	0.784
4112	31.6	19.7	0.528	0.989
*c 4277	16.1	31.1	4.83	4.32E−44
*4345	25.4	30.4	1.78	0.00302
4496	17.4	14.9	0.777	0.918
4540	21.9	17.5	1.08	0.303
4983	23.9	27	1.3	0.0242
5011	46.6	26.5	0.315	1
5019	16.8	15.4	1.12	0.27
*c 5072	13.2	185	432	0
*c 5185	56.4	331	48.9	0
*5273	22.6	4300	34700	0
5384	20.4	15.1	0.452	0.994
5447	955	51.8	0.003	1
5534	49.5	33.4	0.44	0.99
5544a	30.1	34.1	1.3	0.06
*5544b	21.2	33.5	2.15	0.0017
*5553	20	8880	1.75E5	0
5568	11.2	11.3	1.06	0.371
5868	12.3	10.8	0.954	0.615
5914	23.9	15.9	0.456	1
5933	67.7	64.9	0.665	0.986
*c 5968	9.23	31	12.3	4.62E−39
6171	14.5	11.2	0.479	0.998
6458	17.7	14.3	0.602	0.997
6623	11.5	13.2	1.15	0.183
6806	14.3	14.9	1.22	0.168
6869	11.7	15	1.46	0.024
*7061	88.5	129	1.99	5E−7
7462	13.3	12.2	0.794	0.824
7503	14.1	18.8	1.28	0.0674
*c 7504	14.2	29.4	5.82	2.32E−84
7602	12.1	13.2	1.16	0.149
7672	19.5	15.9	0.728	0.96

TABLE 4—*Continued*

Star (HR)	Expected rms[b] (m s^{-1})	Observed rms[c] (m s^{-1})	χ^2_v	False Alarm
8085	15.3	10.6	0.505	1
8086	15	11.1	0.694	0.961
8314	42.1	33.8	0.705	0.904
8382	12	7.77	0.565	0.938
8665	47.1	26.9	0.29	1
*c 8729	12.5	40.5	14.8	0
8832	12.4	13.4	0.931	0.602
8969	25.8	23.7	0.674	0.974
Gl 250a.....	12.3	15.1	1.33	0.163
*Gl 641.....	15.7	24	2.8	1.14E−06
*Gl 688.....	9.4	3730	21800	0
Gl 716	16.3	15.8	0.545	0.886

[a] We give the reduced χ^2 either about the mean or from the straight line fit (see § 3.2). We mark with "*" in the leftmost column those stars which show a false alarm probability less than 1%, and with a "c" those with confirmed planetary-mass companions (Table 1).

[b] The predicted rms taking into account the Doppler errors and intrinsic variability.

[c] The observed rms of the velocities after subtraction of the mean or straight line.

1997; Table 1). The duration of these observations is 1.2 yr. By chance, most of the measurements lie above the zero point of the orbit, giving a 20 m s^{-1} difference between the mean of the data and the correct zero point. We plot the best-fit sinusoid with a fixed mean as a dashed line and with a floating mean as a solid line. The traditional periodogram does not detect a significant period; it identifies a period of 43.9 days, but with false alarm probability 8%. The floating-mean periodogram gives a very significant detection at the correct period of 40.0 days (see Table 5). *Thus allowing the mean to float is not only important at long periods but is also crucial to account for statistical fluctuations when the number of observations is small.* A similar situation could occur owing to uneven sampling. If a sinusoid is sampled at nearly the same phase each cycle (e.g., for $P \approx 1$ yr), the mean of the data could be significantly different from the zero point of the sinusoid, and the periodicity thus go undetected.

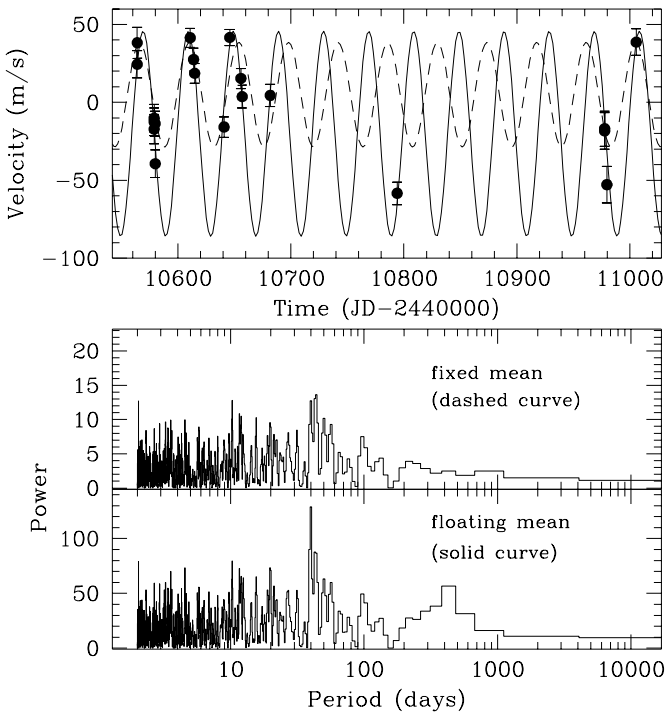

FIG. 4.—Further example of traditional vs. floating-mean periodogram. The star HR 5968 has a companion with $K = 67$ m s^{-1} and $P = 39.6$ days (Noyes et al. 1997; Table 1). The upper panel shows our 20 radial velocity measurements of HR 5968, spanning 1.2 yr. The dashed curve shows the best-fit sinusoid ($P = 43.9$ days) that we obtain after subtracting the mean of the data. The solid curve ($P = 40.0$ days) is the result of fitting the sinusoid and mean simultaneously. The rms of the residuals to the dashed curve is 20 m s^{-1}; for the solid curve, it is 8 m s^{-1}, exactly what we would predict from intrinsic variability and measurement errors. The lower panel shows the periodogram obtained in each case. To allow for a fair comparison, the vertical scales have a ratio of $(20/8)^2$ to account for the different normalization factors.

If the number of data points is large and the periodicity is well sampled, the mean of the data does give a good estimate of the correct zero point. *However, the traditional periodogram fails in precisely the regime where we require it to be robust; namely, when the number of observations is small, the duration of the observations is limited, or the sampling uneven.* For this reason, we adopt the floating-mean periodogram, despite its being less computationally efficient than the simple Lomb-Scargle formula.

Following Walker et al. (1995), we make a further generalization in the case where we subtract a straight line from the data (those stars marked * in Table 3). In this case we must fit a sinusoid plus a straight line to the data at each frequency (i.e., add a term $\propto t_j$ to eq. [5]). For these stars, we use χ^2_{N-2} in place of χ^2_{N-1} in our definition of the periodogram and replace $\chi^2(\omega)$ by the χ^2 from the straight line plus sinusoid fit. This gives a general formula for the floating-mean periodogram power (as Walker et al. 1995, eq. [A2])

$$z(\omega) = \frac{(N - m - 2)}{2} \frac{\chi^2_{N-m} - \chi^2_{N-m-2}(\omega)}{\chi^2_{N-m-2}(\omega_0)}, \qquad (7)$$

where $m = 1$ for a mean or $m = 2$ for a straight line. Comparing equation (7) with equation (4), we see that the periodogram is similar to the F-statistic, measuring how much the fit is improved by introducing the two extra sinusoid parameters.

3.4. *Application of the Periodogram*

3.4.1. *Search for Periodicities*

For each star, we plot the periodogram and look for the frequency that gives the maximum power $z_{\max}$. The perio-

TABLE 5

PERIODOGRAM RESULTS[a]

STAR (HR)	z_{max}	FALSE ALARM PROBABILITY			PERIOD (days)	K (m s^{-1})
		Gaussian	Mixed	Analytic[b]		
8	14.2	0.1	0.1	0.0539	6.31	15.1
88	15	0.03	0.03	0.0154	3.1	31.8
166	13.9	0.04	0.03	0.0135	4.01	7.25
219a	11	0.33	0.76	0.19	6.4	6.72
222	9.93	0.34	0.28	0.288	7.9	8.43
*c 458	38.2	<0.0025	<0.0025	6.2E−10	4.62	64.4
493	16.2	0.03	0.1	0.00993	7.89	6.62
*509	35.4	<0.0025	<0.0025	5.95E−11	19.5	4.1
582	12.4	0.28	0.2	0.174	11000	22.1
753	8.32	0.63	0.63	0.77	2.27	7.06
799	15.9	0.06	0.06	0.0366	15.5	11.7
857	23.5	0.0175	0.03	0.00253	8.26	36.7
*937	18	<0.0025	0.0125	0.000479	1920	5.73
962	16.3	0.08	0.28	0.044	3.28	28.6
*996	40.9	<0.0025	<0.0025	4.71E−09	46.9	28.7
*1084	36.1	<0.0025	<0.0025	1.35E−09	2520	14.7
1101	10.3	0.42	0.49	0.36	3.73	8.35
1262	12.2	0.4	0.34	0.398	19	19.2
1325	16.1	0.015	0.207	0.00232	5.39	8.2
1614	9.93	0.34	0.67	0.283	92.6	5.2
*1729	59.1	<0.0025	<0.0025	0	376	8.12
1925	45.1	0.0175	0.12	0.000584	3.2	85.7
*2047	498	<0.0025	<0.0025	0	11000	3410
2483	12.6	0.11	0.2	0.0585	6.89	10.5
2643	9.88	0.36	0.2	0.35	3640	14.4
3262	13.2	0.09	0.15	0.0619	2.54	16.4
*c 3522	978	<0.0025	<0.0025	0	14.6	75.9
3538	9.43	0.58	0.62	0.625	4.89	10.3
3625	18.4	0.01	0.05	0.0083	29.1	24.1
3881	13	0.04	0.02	0.0347	15.6	7.57
*3951	15.6	0.005	0.0625	0.00323	6.4	7.57
4112	13.2	0.15	0.13	0.0633	8.84	17.5
*c 4277	456	<0.0025	<0.0025	0	1070	46.4
*4345	26.1	<0.0025	0.0025	0.000289	2.96	33.5
*4496	21.6	<0.0025	<0.0025	4.95E−05	2.03	11.7
*4540	27.1	<0.0025	<0.0025	8.9E−07	10.7	14.8
*4983	27.7	<0.0025	<0.0025	3.87E−07	352	24.8
5011	14.3	0.09	0.04	0.0298	2.23	25.4
*5019	29.6	<0.0025	0.11	2.88E−06	3550	14.6
*c 5072	304	<0.0025	<0.0025	0	117	252
*c 5185	387	<0.0025	<0.0025	0	3.31	456
*5273	62.4	<0.0025	<0.0025	1.24E−06	3300	4130
5384	10.4	0.35	0.45	0.336	14.9	8.83
5447	19.3	0.0125	0.0075	0.00222	2.08	50.2
5534	11.3	0.71	0.79	0.805	2.88	35.1
*5544a	20.1	0.0025	0.0375	0.000672	3.78	26.6
5544b	14.4	0.38	0.57	0.313	9.9	29
5553	28.7	0.02	0.177	0.00546	126	10500
*5568	18.6	<0.0025	<0.0025	0.00091	4.06	9.67
5868	13.9	0.01	0.07	0.0123	358	6.06
5914	14	0.02	0.2	0.0107	39.6	7.52
5933	15.7	0.01	0.223	0.00498	9.04	45.9
*c 5968	129	<0.0025	<0.0025	1.89E−08	40	65.7
6171	12.7	0.07	0.05	0.0566	2.14	10.3
6458	13	0.04	0.34	0.0271	11000	16.1
*6623	36.2	<0.0025	<0.0025	2.07E−08	11000	55
6806	12.8	0.11	0.15	0.0561	32	8.83
6869	13	0.08	0.28	0.0314	4.81	8.03
*7061	17.4	0.005	0.0025	0.00173	5.32	94.4
7462	10.2	0.25	0.16	0.178	16.9	7.42
7503	11.6	0.19	0.19	0.141	11000	24.9
*c 7504	101	<0.0025	<0.0025	0	770	29.3
*7602	45.3	<0.0025	0.08	4.59E−11	4730	12.7

TABLE 5—*Continued*

Star (HR)	z_{max}	False Alarm Probability			Period (days)	K (m s^{-1})
		Gaussian	Mixed	Analytic[b]		
*7672	18.9	<0.0025	0.107	0.000611	3.19	15
8085	13.9	0.02	0.1	0.00822	2.22	4.55
*8086	20.3	<0.0025	0.03	0.000368	19	8.58
8314	17.6	0.03	0.12	0.0131	2.68	35.8
8382	9.79	0.46	0.66	0.486	6.19	5.81
8665	12.1	0.16	0.28	0.111	42.8	22.4
*c 8729	4440	<0.0025	<0.0025	0	4.23	56.2
8832	16.7	0.0175	0.307	0.00601	11000	101
8969	8.36	0.57	0.26	0.61	4	11.7
Gl 250a.....	23.8	0.05	0.06	0.0192	20.7	15.1
Gl 641	18.9	0.0125	0.02	0.0116	6.33	33.7
Gl 688	269	0.16	0.21	0.104	2.36	6370
Gl 716	7.21	0.65	0.92	0.904	3.27	19.6

[a] A "*" in the leftmost column indicates those stars with a periodicity significant at the 1% level. A "c" indicates those stars with confirmed planetary-mass companions (Table 1).

[b] Determined by fitting for the number of independent frequencies using the analytic distribution given in Table 9. A "0" means infinitesimal false alarm probability.

dogram power z is a continuous function of frequency $f = \omega/2\pi$. However, the finite duration of the observations T gives each periodogram peak a finite width $\approx 1/T$. Thus in a frequency range Δf, there are roughly $T\Delta f$ peaks. To make sure we sample all the peaks, we evaluate $4T\Delta f$ periods between 2 days and 30 yr.[8] Monte Carlo tests indicate that this gives adequate sampling of the periodogram. We evaluate z at evenly spaced frequencies using a linear least-squares fitting algorithm from Press et al. (1992).

To assess the significance of a possible detection, we test the *null hypothesis* that the data are pure noise. We ask, what is the false alarm probability associated with z_{max}, or how often would noise fluctuations conspire to give a maximum power larger than that observed? We use Monte Carlo tests to find the false alarm probability.[9] For each star, we make fake data sets of either a mean or straight line plus noise. We then perform the same analysis as for the original data. We find the maximum periodogram power and ask, in what fraction of trials does z_{max} exceed the observed value? This fraction is the false alarm probability.

We add noise to the simulated data sets in two ways. One is to add Gaussian deviates with the same variance as the observed velocities, keeping the same relative weights and observation times. The second is to take the observed velocities and randomize them, keeping the sample times fixed (the so-called bootstrap method; Press et al. 1992). In this case, we randomize the pre-fix and post-fix velocities separately, to account for their different v/σ distributions. We find that both approaches give false alarm probabilities that are similar for most stars. We have also applied the analytic distribution given in Appendix B to our results (see Table 9) and fitted for the number of independent frequencies M. The resulting analytic false alarm probabilities agree well with our Monte Carlo calculations.

The results are given in Table 5. For each star, we give the maximum power z_{max}, the corresponding best-fit period and velocity amplitude, and the false alarm probabilities determined from 400 Monte Carlo trials for each star. We mark with * those stars which show false alarm probabilities less than 1%. Apart from those stars with confirmed companions (Table 1), these are HR 509, HR 937, HR 996, HR 1084, HR 1729, HR 2047, HR 3951, HR 4345, HR 4496, HR 4540, HR 4983, HR 5019, HR 5273, HR 5544a, HR 5568, HR 6623, HR 7061, HR 7602, HR 7672, and HR 8086. Again, our motivation for choosing a 99% detection threshold is that we then expect no more than one false detection in our sample of 76 stars.

We find that 20 stars have more than one peak in the periodogram with false alarm probability less than 1%. The search for multiple companions is beyond the scope of this paper; however, we carried out a simple test of whether these secondary peaks were due to aliasing of the primary period by the finite sampling. We subtracted off the best-fit sinusoid from the data and looked at a periodogram of the residuals to see if the secondary peaks remained. Only in two cases did they remain: HR 458, which has a second peak at 1210 days, and HR 509, which has a second peak at 60 days.

3.4.2. *Variability*

The *average* power $\bar{z}$ (averaged over frequency) is an additional indicator of variability. If the data are drawn from a Gaussian distribution, we expect the mean power to be $\bar{z} \approx 1$ (the mean value of the F-distribution). Again using a Monte Carlo method, we calculate the false alarm probability associated with the observed $\bar{z}$. Namely, we ask in what fraction of simulated data sets is the mean power larger than the observed value? A low false alarm probability in this test indicates either a periodicity may be present (the uneven sampling results in "leakage," which contaminates the background level), some non-Gaussian behavior,

[8] The "average" Nyquist period of our observations ($P_{Nyq} \approx 2T/N$) is a few months. However, the uneven sampling gives information on much shorter periods (perhaps much shorter than the minimum spacing between observations; see Eyer & Bartholdi 1998). The minimum period we investigate is 2 days. The maximum period of 30 yr is a few times greater than the typical duration of the observations.

[9] The false alarm probability increases as the frequency range searched Δf increases (Schwarzenberg-Czerny 1996, 1997a, 1998 refers to this as the *bandwidth penalty*). As we discuss in Appendix B, although the distribution of z at one particular frequency is easy to write down analytically, the number of independent frequencies in a frequency range Δf is not. For this reason, we adopt a Monte Carlo approach. This also allows us to check for non-Gaussian effects.

or some kind of "broadband" variability (for example as might be expected from magnetic activity). The results are shown in Table 6. Several stars show significantly high $\bar{z}$ at the 99% level. Apart from those stars with confirmed companions (Table 1), they are HR 88, HR 166, HR 509, HR 937, HR 996, HR 1084, HR 1729, HR 2047, HR 4345, HR 4496, HR 4540, HR 4983, HR 5019, HR 5273, HR 5544a, HR 5568, HR 5868, HR 5914, HR 5933, HR 6623, HR 7061, and HR 7602.

3.5. *Results of Our Search for Companions*

Our sample of 76 stars contains eight stars with companions of planetary mass: HR 3522, HR 4277, HR 458, HR 5072, HR 5185, HR 5968, HR 7504, and HR 8729. All of these companions give highly significant periodogram peaks. The orbital period and velocity amplitude obtained from the periodogram agree well with a Keplerian fit, although not surprisingly, the velocity amplitude is less than that of the Kepler fit for eccentric orbits. The orbital parameters for these planetary-mass companions and references are given in Table 1.

Five stars have companions with $M_p \sin i > 15\ M_J$ that have been reported by previous authors. They are HR 2047 ($M \sin i = 0.15\ M_\odot$, $P = 14.2$ yr; Irwin, Yang, & Walker 1992), HR 5273 ($M \sin i = 0.4\ M_\odot$, $a = 5$ AU; Kamper 1987), HR 5553 ($K \approx 20$ km s^{-1}, $P = 125$ days; Beavers & Salzer 1983), HR 6623 (Cochran & Hatzes 1994 report a slope of -40 ± 5 m s^{-1} yr^{-1}) and Gl 688 ($K = 5.7$ km s^{-1}, $P = 83.7$ days; Tokovinin 1991). These massive companions explain the variability seen in these stars, and the trend in those two, HR 2047 and HR 6623, for which we have not yet seen a complete orbital period. They provide interesting examples of the limitations of the periodogram. There are 20 observations of HR 5553. The orbital period is correctly identified by the periodogram as 125 days, but it is not deemed a significant detection. Gl 688 has only seven observations, and the periodogram is unable even to identify the correct period.

TABLE 6

AVERAGE PERIODOGRAM POWER[a]

STAR (HR)	$\bar{z}$	FALSE ALARM Gaussian	FALSE ALARM Mixed	STAR (HR)	$\bar{z}$	FALSE ALARM Gaussian	FALSE ALARM Mixed
8	2.12	0.05	0.07	*5019	4.92	<0.0025	0.02
*88	2.62	<0.0025	<0.0025	*c 5072	19.2	<0.0025	<0.0025
*166	1.98	<0.0025	0.01	*c 5185	22.6	<0.0025	<0.0025
219a	1.4	0.39	0.71	*5273	9.92	<0.0025	0.02
222	1.63	0.26	0.12	5384	2.35	0.15	0.2
*c 458	3.66	<0.0025	<0.0025	5447	3.12	0.0025	0.0025
493	2.33	0.09	0.11	5534	2	0.55	0.63
*509	2.75	<0.0025	<0.0025	*5544a	3.29	<0.0025	<0.0025
582	1.62	0.43	0.39	5544b	3.64	0.12	0.24
753	1.32	0.63	0.42	5553	4.35	0.04	0.198
799	2.26	0.04	0.02	*5568	2.7	<0.0025	0.0025
857	4.71	0.0125	0.0075	*5868	1.84	<0.0025	0.03
*937	1.95	<0.0025	<0.0025	*5914	1.94	<0.0025	0.07
962	2.13	0.19	0.42	*5933	2.4	<0.0025	0.04
*996	8.04	<0.0025	<0.0025	*c 5968	19.9	<0.0025	<0.0025
*1084	3.37	<0.0025	<0.0025	6171	1.7	0.27	0.15
1101	1.8	0.33	0.39	6458	1.49	0.18	0.35
1262	1.75	0.53	0.32	*6623	2.99	<0.0025	0.04
1325	2.7	0.0175	0.237	6806	2.94	0.02	0.02
1614	2.03	0.14	0.54	6869	2.69	0.02	0.1
*1729	4.47	<0.0025	<0.0025	*7061	2.56	<0.0025	<0.0025
1925	16.5	0.005	0.125	7462	1.69	0.26	0.09
*2047	54.6	<0.0025	<0.0025	7503	1.56	0.22	0.12
2483	1.86	0.05	0.11	*c 7504	6.6	<0.0025	<0.0025
2643	1.15	0.72	0.3	*7602	7.05	<0.0025	<0.0025
3262	1.74	0.07	0.15	7672	2.5	0.0025	0.0075
*c 3522	51.6	<0.0025	<0.0025	8085	2.26	0.01	0.02
3538	1.64	0.53	0.63	8086	3.09	0.0025	0.005
3625	3.07	0.01	0.04	8314	2.8	0.01	0.14
3881	1.44	0.2	0.12	8382	2.31	0.27	0.51
3951	2.51	0.0025	0.0025	8665	1.74	0.14	0.26
4112	2.46	0.11	0.04	*c 8729	248	<0.0025	<0.0025
*c 4277	19.1	<0.0025	<0.0025	8832	2.15	0.05	0.0675
*4345	4.54	<0.0025	<0.0025	8969	1.22	0.51	0.11
*4496	2.59	<0.0025	<0.0025	Gl 250a	3.81	0.14	0.05
*4540	5.31	<0.0025	<0.0025	Gl 641	3.04	0.02	0.01
*4983	4.13	<0.0025	<0.0025	Gl 688	104	0.18	0.22
5011	2.43	0.03	0.02	Gl 716	1.44	0.76	0.96

[a] Here we give the mean periodogram power $\bar{z}$ evaluated by summing all the powers evaluated in a periodogram and dividing by the number of frequencies. We mark with a "*" those stars with false alarm probability less than 1%. A "c" indicates those stars with confirmed planetary-mass companions (Table 1).

Seven stars have significant long-term trends, the slopes of which are given in Table 7. These are HR 219a, HR 753, HR 1325, HR 5544a, HR 5544b, HR 7672, and HR 8086. Long-term trends such as these most likely indicate a companion with $a \gtrsim 10$ AU and $M_p \sin i > 15\ M_J$. Of course many of the other slopes listed in Table 3 may also be due to companions of lower mass (but still with periods $P \gg 11$ yr). The slopes of HR 5544a and HR 5544b are of almost the same magnitude but opposite sign, as expected for orbiting companions. HR 8086 is an interesting case because much of its slope is due to secular acceleration, a geometrical effect that stems from the exchange of proper motion for radial velocity. This effect is negligible for the other stars in our sample, but we see it for HR 8086 because it is close and has a large velocity relative to us. Secular acceleration also explains why we do not see a corresponding negative slope in HR 8085, the companion to HR 8086.

The 20 remaining stars that show significant variability or periodicities are listed in Table 7. These stars are candidates for having planetary-mass companions. We include those stars with a significant periodicity, and those without a significant periodicity but with variability in excess of our prediction of § 2.1. We have divided these stars into two groups, chromospherically active ($P_{\rm rot} \leq 14$ days) and chromospherically quiet ($P_{\rm rot} > 14$ days). The best-fit velocity amplitudes for the chromospherically quiet stars are of order the predicted scatter in the velocities owing to Doppler errors and intrinsic variability. This makes it difficult, even for very significant periodogram peaks, to identify confidently the observed velocity variations with the Keplerian orbit of a companion. For the chromospherically active stars ($P_{\rm rot} \leq 14$ days), there is an additional complication. Even though we account for the excess variability expected in chromospherically active stars, intrinsic velocity variations are likely to be periodic on many different timescales. This renders periodicities seen in these stars suspect, as they may be related to the rotation period, convective motions, or magnetic activity. Thus, despite having

TABLE 7

STARS WITH SIGNIFICANT VARIABILITY OR PERIODICITIES[a]

		VARIABILITY[c]		PERIODOGRAM[d]				
STAR	SLOPE[b] (m s^{-1} yr^{-1})	χ^2	$\bar{z}$	Period (days)	K (m s^{-1})	$\sigma_{\rm exp}$ (m s^{-1})	$\sigma_{\rm rms}$ (m s^{-1})	$P_{\rm rot}$ (days)
Stars with Significant Slopes								
HR 219a	9.3±0.6	...	...	...	...	...	...	15
HR 753	12±0.7	...	...	...	...	...	...	48
HR 1325	5±0.5	...	...	...	...	...	...	43
HR 5544a	18±1.1	...	*	3.8	27	30	26	6
HR 5544b	−25±1.2	*	...	...	...	...	...	11
HR 7672	−24±0.6	...	...	3.2	15	20	11	14
HR 8086	8.9 ± 0.6	...	...	19	8.6	15	6.7	38
Chromospherically Inactive Stars ($P_{\rm rot} > 14$ days)								
HR 166	...	*	*	...	...	...	...	44
HR 509	...	...	*	20	4.1	14	6.0	34
HR 937	...	...	*	5.3[e]	5.7	17	8.2	21
HR 1729	...	...	*	376	8.1	13	5.9	24
HR 3951	...	...	*	6.4	7.6	12	7.6	27
HR 4496	...	...	*	2.0	12	17	9.2	17
HR 5019	...	...	*	9.8[e]	15	17	7.6	29
HR 5568	...	...	*	4.1	9.7	11	7.1	40
HR 5868	...	...	*	...	...	...	...	26
HR 5914	...	...	*	...	...	...	...	15
HR 7602	...	...	*	13[e]	13	12	5.5	52
Chromospherically Active Stars ($P_{\rm rot} \leq 14$ days)								
HR 88	...	*	*	...	...	...	...	8
HR 996	...	...	*	47	29	23	16	9
HR 1084	...	...	*	6.9[e]	15	20	13	12
HR 4345	...	*	*	3	34	25	20	8
HR 4540	...	...	*	11	15	22	12	14
HR 4983	...	...	*	352	25	24	18	12
HR 5933	...	...	*	...	...	...	...	3
HR 7061	...	*	*	5.3	94	89	102	2
Gl 641	...	*	...	...	...	...	...	11

[a] We do not include those stars with confirmed planetary mass companions (listed in Table 1), or those with stellar or substellar companions (HR 2047, HR 5273, HR 5553, HR 6623, and Gl 688; see § 3.5).

[b] The best-fit slope for those stars with significant trends greater than 5 m s^{-1} (Table 3, § 3.1).

[c] A "*" indicates a star with significant variability according to the χ^2 test (Table 4, § 3.2) or the $\bar{z}$ test (Table 6, § 3.4).

[d] For those stars with significant periodicities (Table 5, § 3.4), we give the period and velocity amplitude K of the best-fit sinusoid, $\sigma_{\rm exp}$, the predicted rms taking into account Doppler errors and intrinsic variability, and $\sigma_{\rm rms}$, the rms of the residuals to the best-fit sinusoid.

[e] Units: years.

extremely low false alarm probabilities in the periodogram analysis, none of the periodicities listed in Table 7 are convincing as companions. We are currently making more observations of these stars to attempt to confirm or rule out these periodicities.

4. UPPER LIMITS ON COMPANION MASS

For those stars without a confirmed companion, we would like to know the upper limit on the signal amplitude K. In this section, we use the periodogram to place upper limits on the velocity amplitude as a function of period. Strictly, our upper limits are on the amplitude of *circular orbits* because we assume a sinusoidal periodicity. However, we expect our upper limits would not be significantly different for eccentric orbits. This is because for a given period, eccentric orbits have a larger velocity amplitude K, but an extended duration of roughly constant velocity near apastron. These two effects will cancel each other to some extent for a companion of given mass and orbital radius. Of course, this is not true for orbital periods longer than the duration of the observations, for which our upper limits are strictly for circular orbits. We first describe our method in detail and then present our upper limits on companion mass as a function of orbital radius for each star in the survey.

4.1. *Method*

Our method for placing upper limits uses the fact that, because of measurement errors, different observations of the same signal give different periodogram powers. Most of the time, a large signal amplitude will give a large power. Sometimes, because of noise fluctuations, a large signal will give a small power, but less and less often as the signal amplitude increases. This means that, given a particular observation, we can rule out very large signal amplitudes because they have a very small chance of giving a power as small as the observed value.[10] We define the 99% upper limit to be the signal amplitude such that the periodogram power would be less than or equal to the observed value only 1% of the time.

We proceed as follows. For each star, we find the maximum periodogram power $z_{\max}$ from the data (as given in Table 5) for periods between 2 days and 30 yr. Then for different trial frequencies, we make simulated data sets of a sinusoid (with frequency ω, amplitude K, and randomly selected phase ϕ) and noise. We find the periodogram power $z(\omega)$ for each simulated data set and ask how often is z larger than the observed value $z_{\max}$? The 99% upper limit to the velocity amplitude at frequency ω is that K which gives $z > z_{\max}$ in 99% of trials. In other words, the observed $z_{\max}$ lies at the lowest 1 percentile of the distribution of z that stems from the upper limit to the velocity.

For each trial, we evaluate the periodogram at only one frequency, the trial frequency ω. This assumes that the maximum periodogram power will occur at the trial frequency. We have tested this assumption by evaluating the upper limits using 100 frequencies centered on the trial frequency, with the same spacing as used in the periodogram. The upper limits from both methods agree well, and hence we adopt the former as it is computationally faster.

To add noise to the simulated data sets, *we utilize the residuals to the sinusoid that best fits the data* (i.e., the residuals after subtracting from the data the sinusoid corresponding to the maximum periodogram power $z_{\max}$). We motivate this in Appendix B, where we show that, if the data consist of a sinusoid plus noise, the best estimate of the noise variance is the variance of the residuals to the best fit sinusoid. This allows us to obtain the noise variance directly from the data, without having to rely on the estimated errors of § 2.1. We find that the variance of the residuals is typically less than the estimated error by a factor of 1.5, consistent with our finding that we overestimated the internal errors (see § 2.1). We are thus confident that the residuals give a good estimate of the noise variance for each star.

For each observation, we add noise by selecting at random from the v/σ distribution of the residuals, scaling by the expected variability σ_j for each data point. When choosing at random, we select from the pre-fix and post-fix data separately, as appropriate. We have also tried adding Gaussian noise (with appropriate relative weighting between points), scaling by the variance of the residuals to the best fit sinusoid. The upper limits from the two methods agree to 10% or better.

4.2. *Results*

The 99% upper limits are plotted in the $M_p \sin i$–a plane as a solid line in Figure 5 for each star in the sample. For clarity, we state again the meaning of our upper limit. For each star, we imagine repeating the observations many times, each with identical sampling, errors, and duration as the real observations. The 99% upper limit is the mass ($M_p \sin i$) of a companion that, if present at orbital radius a, would give a periodogram power larger than that observed in the real data ($z_{\max}$) in 99% of our repeated observations. Thus a companion more massive than the upper limit is excluded by the data at better than 99% confidence.

For each star, we calculate the upper limit to the velocity amplitude at 500 logarithmically spaced periods between 2 days and 30 yr. To convert velocity and period (K, P) to mass and orbital radius ($M_p \sin i$, a), we use equations (1) and (3). We estimate the mass of each star from its spectral type (Table 2) using a simple empirical formula,

$$M/M_\odot = 1.3 - \left(\frac{s}{38}\right) + \frac{3}{10}\left(1 - \frac{s}{30}\right)^5 , \qquad (8)$$

where s parameterizes the spectral type, ranging from $s = 0$ for F0 to $s = 30$ for M0 (for example, $s = 22$ refers to spectral type K2). This formula reproduces Table 9.6 of Lang (1991) to within 10%. Metallicity renders our masses uncertain by a further 10% (see Carney et al. 1994). This is adequate for our purposes, however.

Inspection of the upper limits shows that, for many periods, the upper limit to the velocity amplitude K is roughly independent of period. For each star, we list in Table 8 the average velocity upper limit $\bar{K}$ calculated for periods less than half the duration of the observations ($P < T/2$). We show the corresponding line of constant

[10] This approach to placing upper limits is a "frequentist" one, as discussed by de Jager (1994) (see also Caso et al. 1998), and applied to the Rayleigh test by Protheroe (1987) and Brazier (1994). It was used in searches for pulsations in the quiescent emission from low mass X-ray binaries by Leahy et al. (1983) and Vaughan et al. (1994). In their work, the noise is dominated by photon-counting (Poisson) noise, and the time series is evenly sampled. This allows the noise level to be "read off" the power spectrum, giving a natural normalization (Leahy et al. 1983). This is not true in the case of uneven sampling; hence the different approaches in the literature to normalizing the periodogram (see Appendix B).

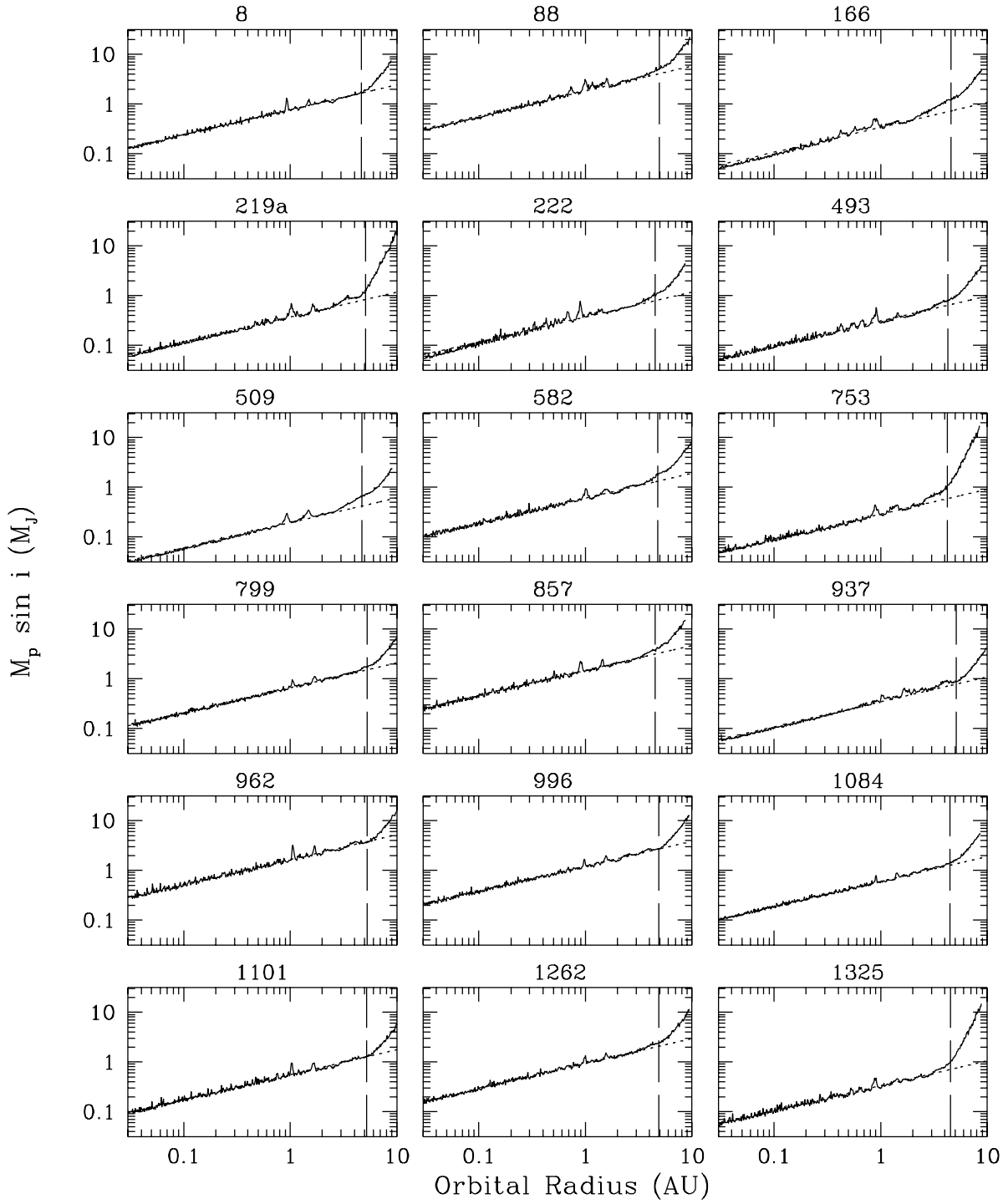

FIG. 5.—The 99% upper limit on the mass (M_p sin i) of a companion in a circular orbit as a function of orbital radius for each of the sample stars. The upper limit is calculated as described in § 4.1. The dotted line shows a line of constant velocity, where the velocity for each star is the mean upper limit given in Table 8. The long-dashed line shows the orbital radius at which the duration of the observations equals the orbital period.

velocity in Figure 5 as a dotted line. The average velocity upper limit is a good estimate of the upper limit for most periods less than the duration of the observations ($\sim$11 yr for most stars; see Table 2).

The upper limit deviates from this "constant velocity" behavior for two reasons. First, the upper limit is larger at periods where the sampling of the observations gives poor phase coverage. For example, many stars show an increase in the upper limit at $a \approx 1$ AU because of the tendency for observations to take place at the same time each year. As expected, these aliasing effects are more important in stars with fewer observations. Second, the upper limit to the velocity amplitude increases for periods greater than the duration of the observations. In Figure 5, we show the orbital radius for which $P = T$ for each star by a vertical dashed line. The upper limit at long periods ($P \gtrsim T$) is sensitive to how we choose the phase in the simulated data sets. The data contain some information about the best-fit phase at each period, but we (conservatively) ignore that and choose the phase at random for each trial.

In Figure 5 we do not show results for the eight stars with confirmed planetary-mass companions (Table 1), or for the

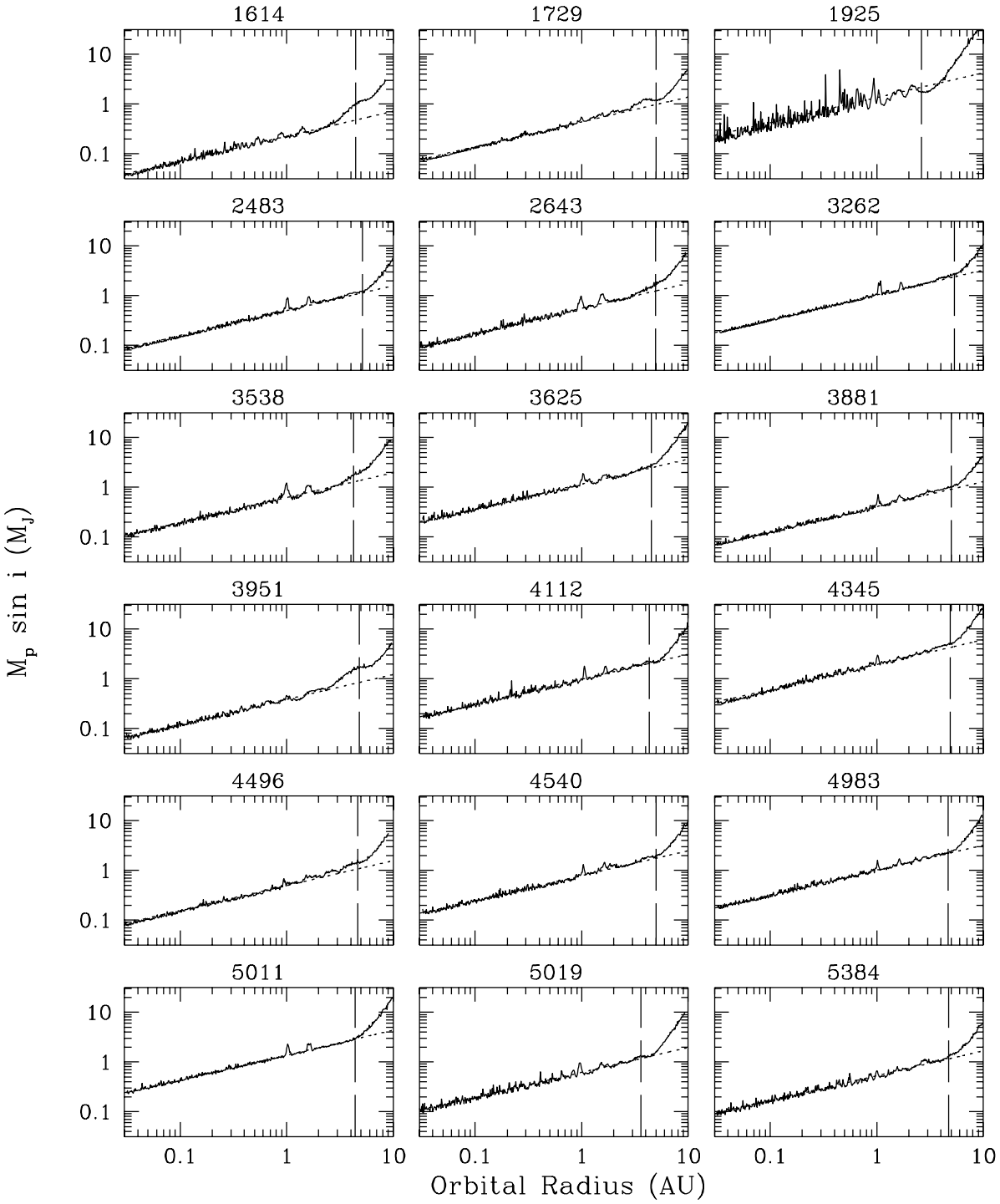

FIG. 5.—*Continued*

five stars with companions with $M_p \sin i > 15\ M_J$ and $P \gtrsim 20$ yr (HR 2047, HR 5273, HR 5553, HR 6623, and Gl 688). An interesting question is whether these stars have second companions. We are currently generalizing our approach to the case of two companions. For now, we note that the residuals to Keplerian fits to the velocities for the five stars with $M_p \sin i > 15$ are less than 30 m s^{-1} in each case. Searches for second companions to the stars with planetary-mass have been made (see Table 1 for references), without success except HR 3522 (ρ^1 55 Cnc) and HR 458 (υ And) show evidence for long period second companions ($P \gtrsim 3$ yr).

Walker et al. (1995, hereafter W95) also used a floating-mean periodogram to place upper limits on companion mass but took a different approach based on subtracting a sinusoid directly from the data.[11] We have applied our method to the data of W95 and find good agreement with their published upper limits. Comparison with their Figure 5 shows that our upper limits on companion mass

[11] This kind of approach to placing confidence limits is discussed by Lampton, Margon, & Bowyer (1976), including the cases where the noise level must be estimated from the data and some of the parameters are "uninteresting" (see also Cline & Lesser 1970, Avni 1976, Cash 1976, and the discussion in Press et al. 1992).

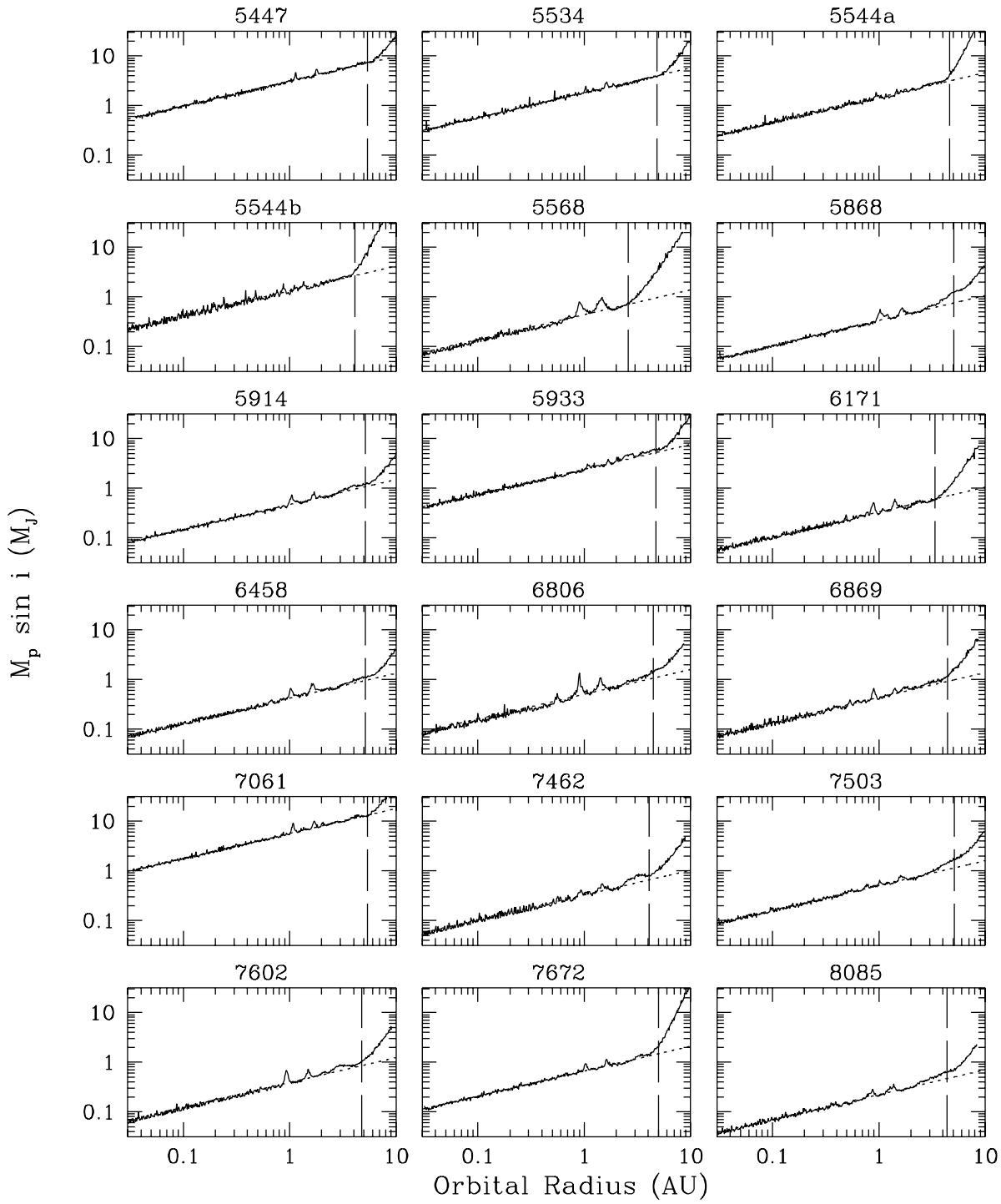

FIG. 5.—*Continued*

are about 10%–20% lower for $P < T$ and 20%–30% higher for $P > T$. In addition, our upper limits, which show less variability from one period to the next, seem less affected by the sampling of the data. The reason for these differences is not clear. Our comparison shows that there is a "theoretical uncertainty" in the upper limits of about 20%. The good agreement of the two techniques, which are quite different, is encouraging.

5. DISCUSSION

So far, we have searched for companions and determined upper limits on the mass of companions for each individual star. We now investigate the implications of our results for the population of planetary-mass companions as a whole.

The observed distribution of the mass and orbital radius of all known planetary mass companions is shown in Figure 6, in which we plot the 17 confirmed companions listed in Table 1 in the M_p sin i–a plane. The dashed lines show constant velocity contours of 10 and 40 m s^{-1} for a 1 $M_\odot$ star. Four features of the observed distribution are interesting. First, all confirmed companions have $K \gtrsim 40$ m s^{-1}. Second, no companions have been detected with orbital

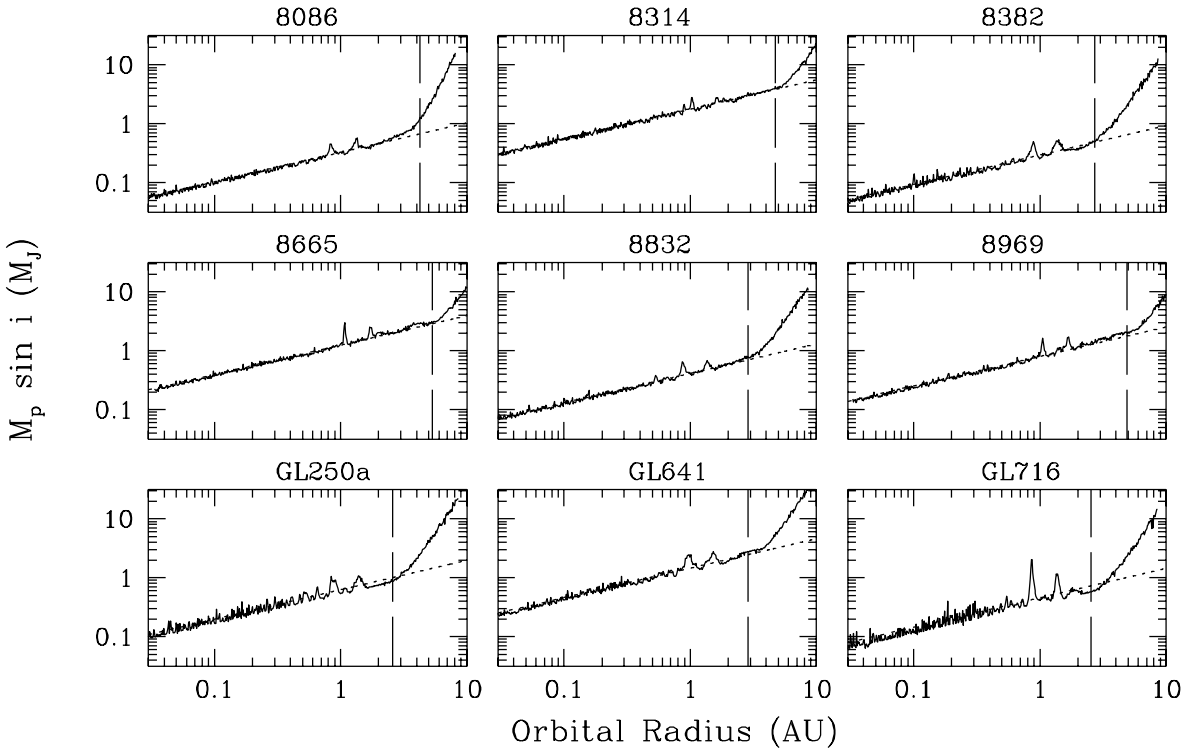

FIG. 5.—*Continued*

radius $a \gtrsim 2.5$ AU. Third, there is a "piling-up" of companions at small orbital radii; for example, of the 17 companions within 2.5 AU, 13 have semimajor axis $a < 0.5$ AU, and five have $a < 0.1$ AU. Fourth, there is a paucity of companions with orbital radii between ~ 0.3 and ~ 1 AU. In this section, we ask whether our results help to explain these features.

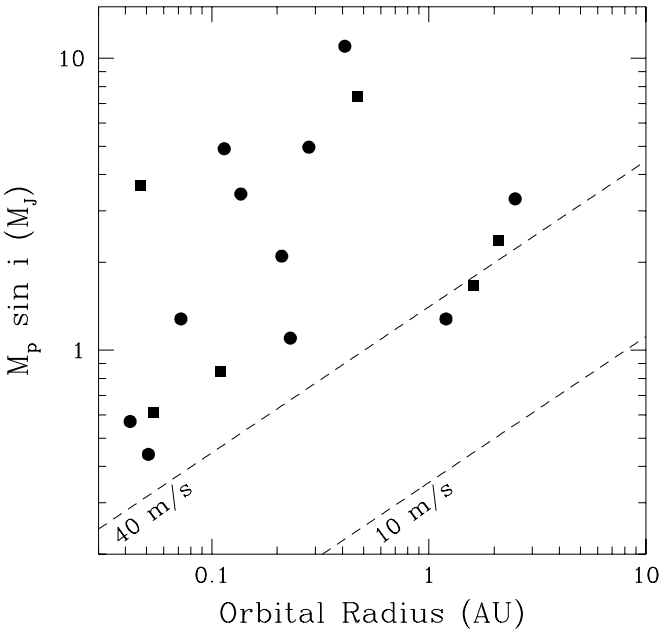

FIG. 6.—Mass (M_p sin i) and orbital radius (semimajor axis for eccentric orbits) of confirmed companions with M_p sin $i < 15\ M_J$. The orbital parameters and references are given in Table 1. Companions discovered at Lick Observatory and included in our sample of stars are shown as solid squares. The dashed lines are lines of constant velocity amplitude for a star with $M = 1\ M_\odot$.

5.1. *Confirmed and Candidate Companions*

First, we summarize the results of our search for companions. We began with a sample of 76 stars from the original Lick Survey. Two stars, HR 5968 (ρ CrB) and HR 8729 (51 Peg) were included in the sample because of the discovery of the companions to these stars by other groups (Table 1) and for this reason cannot be considered part of a statistically unbiased sample. Of the remaining 74 stars, six have confirmed planetary-mass companions, or about 8% of our sample. Our periodogram analysis of § 3.4 reveals several candidate periodicities (marked "$*$" in Table 5 and listed in Table 7), which are yet to be confirmed or ruled out as being due to companions.

We plot the confirmed companions (*circles*) and candidate periodicities (*squares*) in the M_p sin i–a plane in Figure 7. We do this for purely illustrative purposes: *we stress that it may be that none of the candidate periodicities are actually due to companions.* Open and filled squares indicate candidate periodicities for chromospherically active and quiet stars, respectively. The error bars show the 99% upper limit on M_p sin i obtained as described in § 4.1. The dashed lines show constant velocity contours of 5, 10, 20 and 40 m s^{-1} for a 1 $M_\odot$ star.

Inspection of Table 7 shows that there are several candidates for companions with velocity amplitude between the Doppler errors, $K \sim 5$–10 m s^{-1}, and the lowest velocity amplitude detected, $K \sim 40$ m s^{-1}. Thus, one interpretation of our results is that there is an effective detection threshold of $K \approx 40$ m s^{-1}. This could be caused by the fact that confirmation of these low-amplitude orbits is difficult, as we discussed in § 3.5. However, there is an interesting difference in the velocity amplitudes of the candidate periodicities from chromospherically quiet versus chromospherically active stars. Figure 7 shows that there are no candidate periodicities with $K \gtrsim 15$ m s^{-1} in the quiet stars, whereas

TABLE 8

UPPER LIMITS ON THE VELOCITY[a]

Star (HR)	N	σ_{rms}[b] (m s^{-1})	$\bar{K}$ (m s^{-1})	Star (HR)	N	σ_{rms}[b] (m s^{-1})	$\bar{K}$ (m s^{-1})
8.....	41	18	25	4983	100	27	28
88	56	41	53	5011	40	27	38
166	70	12	11	5019	46	15	19
219a.....	69	19	10	5384	29	15	15
222	40	14	12	5447	48	51	73
493	38	8.9	10	5534	24	33	50
509	278	10	6	5544a	60	34	45
582	34	15	17	5544b	23	33	46
753	33	11	9.8	5568	47	11	15
799	43	15	17	5868	106	11	9.2
857	27	25	49	5914	83	16	12
937	131	12	9.4	5933	70	59	61
962	29	30	44	6171	40	11	11
996	67	24	36	6458	72	14	12
1084.....	121	19	20	6806	39	15	17
1101.....	40	15	15	6869	47	15	15
1262.....	30	21	28	7061	78	130	140
1325.....	66	19	11	7462	42	12	10
1614.....	30	7.7	7.7	7503	62	19	14
1729.....	106	9.4	12	7602	85	13	12
1925.....	12	19	44	7672	74	16	18
2483.....	61	14	14	8085	100	11	7.9
2643.....	36	20	16	8086	58	11	12
3262.....	56	22	26	8314	36	34	48
3538.....	32	16	18	8382	21	7.8	9.8
3625.....	28	24	31	8665	61	26	32
3881.....	62	12	11	8832	45	13	14
3951.....	75	11	11	8969	60	24	21
4112.....	35	20	26	Gl 641	29	24	44
4345.....	36	30	53	Gl 250a.....	18	15	21
4496.....	72	15	15	Gl 716	13	16	16
4540.....	80	18	21				

[a] Here we give the mean 99% upper limit on the velocity amplitude $\bar{K}$. For each star, we plot this as a dotted line in Fig. 5. For most stars, it gives a good estimate of the upper limit for periods less than the duration of the observations ($\sim$11 yr for most stars; see Table 2).

[b] The rms of the data for each star. For those stars with a significant long-term trend (§ 3.1), the rms is calculated after subtracting the trend from the data.

all of the candidate periodicities in the active stars have $K \gtrsim 15$ m s^{-1}. Thus another interpretation is that there is a paucity of companions with velocity amplitudes $K \sim 15$–40 m s^{-1}, as none are seen in the subset of quiet stars for which these velocity amplitudes could have been detected. However, we cannot draw conclusions from the present data, as the small number of detections is subject to $\sqrt{N}$ fluctuations.

Figure 7 also shows that there are fewer candidates with orbital radii between $a \sim 0.2$ AU and $a \sim 1$AU than at other orbital radii. If these periodicities are due to intrinsic stellar variations, a possible explanation is that these variations naturally occur on two timescales, the stellar rotation period ($\lesssim$1 month) and the timescale of the magnetic cycle ($\gtrsim$years). However, the apparent paucity of confirmed companions and candidate periodicities between $a \sim 0.2$ AU and $a \sim 1$ AU is interesting and may indicate a real paucity of companions at these orbital radii.

5.2. *Upper Limits and Detectability*

We now turn to the upper limits which we calculated in § 4. In Figure 8, we show a histogram (*left-hand panel*) and cumulative histogram (*right-hand panel*) of the mean velocity upper limits listed in Table 8. For most stars, we can exclude companions with $K \gtrsim 10$–20 m s^{-1} at the 99% level. Nine stars (15% of the sample) have a mean upper limit $\bar{K} < 10$ m s^{-1}, and 38 stars (60% of the sample) have $\bar{K} < 20$ m s^{-1}. About 10 stars have $\bar{K} \gtrsim 40$ m s^{-1}: inspection of Tables 2 and 8 shows that these stars have either a small number of observations, poor internal errors (for example, because they are faint), short rotation period, or a large rms greater than 40 m s^{-1} (for example, because of magnetic activity).

In Figure 9, we plot the cumulative histogram in the M_p sin i–a plane. We take into account the different stellar masses and the effects of sampling (i.e., we use the upper limits as a function of period, Figure 5, rather than just $\bar{K}$; Table 8). The solid lines show contours of the number of stars from which a companion of given mass and orbital radius can be excluded at the 99% level (plotted on a 40 × 40 grid). Each contour is labeled by the number of stars from which we can exclude companions above and to the left of the solid line. The dashed lines show constant velocity contours of 5, 10, 20, and 40 m s^{-1} for a 1 $M_\odot$ star. The filled squares show the six confirmed planetary-mass companions in our sample (Table 1). In Figure 10, we show sections of this contour map. We plot the number of stars from which a companion can be excluded (at the 99% level)

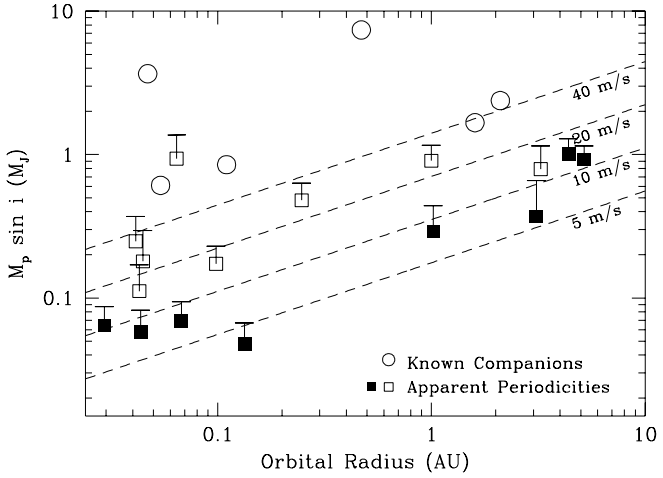

FIG. 7.—Confirmed companions and apparent periodicities from our search for companions, plotted in the M_p sin i–a plane. We plot the six confirmed planetary-mass companions in our sample as circles. The squares show the other significant periodicities revealed by our periodogram analysis (Table 7), presented in this paper for the first time. These periodicities are *as yet unconfirmed* candidates for companions. Open squares indicate chromospherically active stars ($P_{rot} \leq 14$ days); filled squares indicate chromospherically quiet stars ($P_{rot} > 14$ days). The error bar on each point shows the 99% upper limit on the velocity amplitude calculated as in § 4.1. The dashed lines show lines of constant velocity for a solar mass star.

as a function of orbital radius for different masses, and as a function of mass for different orbital radii.

Figure 10 demonstrates the effect of the finite duration of the observations. Even for massive companions (e.g., M_p sin $i > 5$ M_J), the number of stars from which a companion can be excluded decreases rapidly for $a \gtrsim 6$ AU. In Figure 9, we plot with an open circle the point M_p sin $i =$ 1 M_J, $a = 5.2$ AU, or where our solar system would lie in this diagram if sin $i = 1$. This shows that analogs of our solar system are excluded from only a handful of stars once the distribution of sin i is taken into account. This is not true for more massive companions, with M_p sin $i > 3$–4 M_J. Our results show that these companions are not common at orbital radii $a \gtrsim 1$ AU, as found by Walker et al. (1995) in their survey of 21 stars. For example, companions with M_p sin $i > 3$ M_J (>5 M_J) can be excluded from 80% (95%) of our sample of 63 stars.

Our results give some sense of how the detectability of a companion of a particular mass falls off with radius. For example, for M_p sin $i = 1$ M_J (0.5 M_J), the number of stars excluded falls off for $a \gtrsim 0.3$–0.5 AU (0.1 AU). Thus we have detected all companions in the sample with $a \lesssim 0.3$ AU and M_p sin $i \gtrsim 1$ M_J. For the 40 stars with $\bar{K} \lesssim 20$ m s^{-1}, we can exclude 1 M_J companions out to 1 AU, and 2 M_J companions out to 4 AU. Unfortunately, we cannot assume that the detectability of companions is the same in other surveys. Thus we must restrict our attention to the six companions in our sample.

We have performed a simple test of whether the six companions in our sample could have been drawn from a parent population that is uniformly distributed in orbital radius. First, we assume that the mass distribution of companions is uniform in log M_p sin i between 0.1 and 4 M_J. This seems consistent with the observed distribution of M_p sin i (at least for small orbital radii where detectability is good). We select companions at random from this mass distribution and a uniform distribution in orbital radius from 0 to 2.5 AU. We assign the companion to a star in the sample at random, simulate observations of the star using the observation times and errors from the real data, and ask whether the periodogram power is larger than that observed. The "corrected" orbital radius distribution is then the distribution of orbital radii of those companions which give periodogram powers larger than the observed values. We then use the Kolmogorov-Smirnov (KS) test (Press et al. 1992) to find the probability that the six companions are drawn from this "corrected" distribution.

We find that the probability that the six companions are drawn from a parent population with a uniform distribution in orbital radius is $\approx$10%. If we do not include 70 Vir,

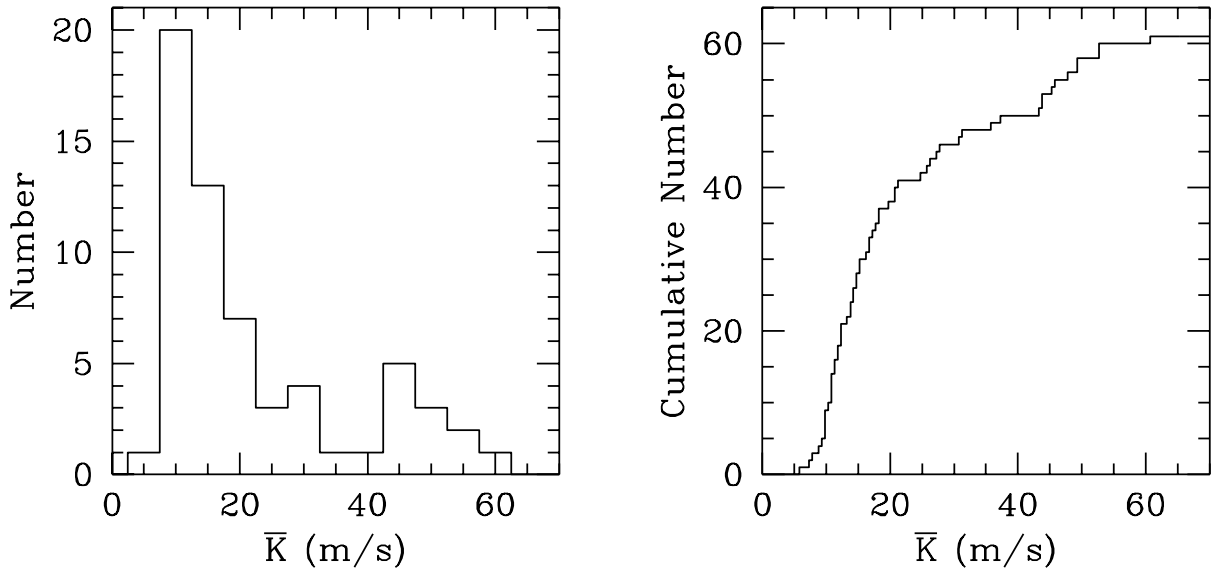

FIG. 8.—Distribution of the mean 99% upper limits on velocity amplitude listed in Table 8. The left-hand panel shows a histogram of the mean upper limits (in 5 m s^{-1} bins; two stars have $\bar{K} > 70$ m s^{-1}). The right-hand panel shows the cumulative distribution of mean upper limits. The total number of stars is 63.

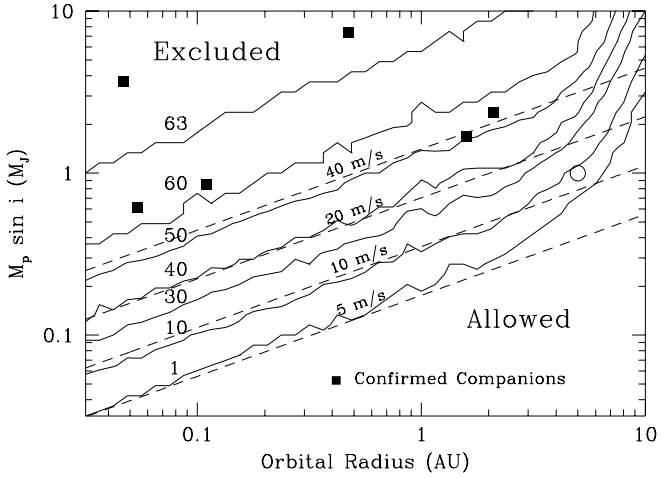

FIG. 9.—Contours of the number of stars for which a companion of particular M_p sin i and a can be excluded at the 99% level, for the set of 63 stars shown in Fig. 5. The contours (*solid lines*) are plotted on a 40 × 40 grid and are labeled with the number of stars excluded from the region up and to the left of the line. We plot as squares those confirmed companions (Table 1) discovered at Lick. Dashed lines give 5, 10, 20, and 40 m s^{-1} constant velocity lines for a 1 $M_\odot$ star. This figure is a two-dimensional version of the right-hand panel of Fig. 8. The circle shows M_p sin i = 1 M_J, a = 5.2 AU.

which may have a low sin i and thus a mass greater than 15 M_J, the probability is 5%. *Thus we cannot rule out that the distribution of companions is uniform in radius.* Also, we emphasize again that we are dealing with a small number of detections that are subject to $\sqrt{N}$ fluctuations. Future detections will enable us to use the KS test in this way to rule out distributions in mass and orbital radius. For now, without knowledge of the detection thresholds of other surveys, we cannot rule out the possibility that the "pile-up" of companions at low orbital radius or the lack of companions between ~0.2 and ~1 AU are due to selection effects or small number statistics.

6. SUMMARY AND CONCLUSIONS

We have presented an analysis of 11 yr of precision Doppler velocity measurements of 76 G-, K-, and F-type stars from the Lick radial velocity survey. We have performed tests for variability, long-term trends, and periodicities. Our sample contains eight confirmed planetary-mass companions, six of which were discovered at Lick, and five companions of stellar or substellar mass (§ 3.5). Seven stars have significant long-term trends, likely indicating a companion with $a \gtrsim 10$ AU and M_p sin $i > 15$ M_J, and 20 stars show variability or periodicities which may indicate a planetary-mass companion (Table 7). We are currently making more observations of these stars to attempt to confirm or rule out these periodicities. For those stars without a confirmed companion, we have calculated upper limits to the mass of a companion as a function of orbital radius (Fig. 5). For most stars, the mean limit on the velocity amplitude is between 10 and 20 m s^{-1} or 0.35 and $0.7M_J(a/\mathrm{AU})^{1/2}$ (for stellar mass $M \approx M_\odot$).

We have searched for periodicities and placed upper limits using a "floating-mean" periodogram, in which we fit sinusoids to the data, allowing the zero point of the sinusoid to "float" during the fit. Allowing the mean to float is crucial to account for statistical fluctuations in the mean of a sampled sinusoid. The traditional Lomb-Scargle periodogram fails when the number of observations is small, the sampling is uneven, or the period of the sinusoid is comparable to or greater than the duration of the observations. This may lead to missed detections or inaccurate upper limits. We have also expanded on the recent discussion by Schwarzenberg-Czerny (1997a, 1997b, 1998) of the correct way to normalize the periodogram and the resulting distribution of periodogram powers. The three different prescriptions in the literature for normalizing the periodogram

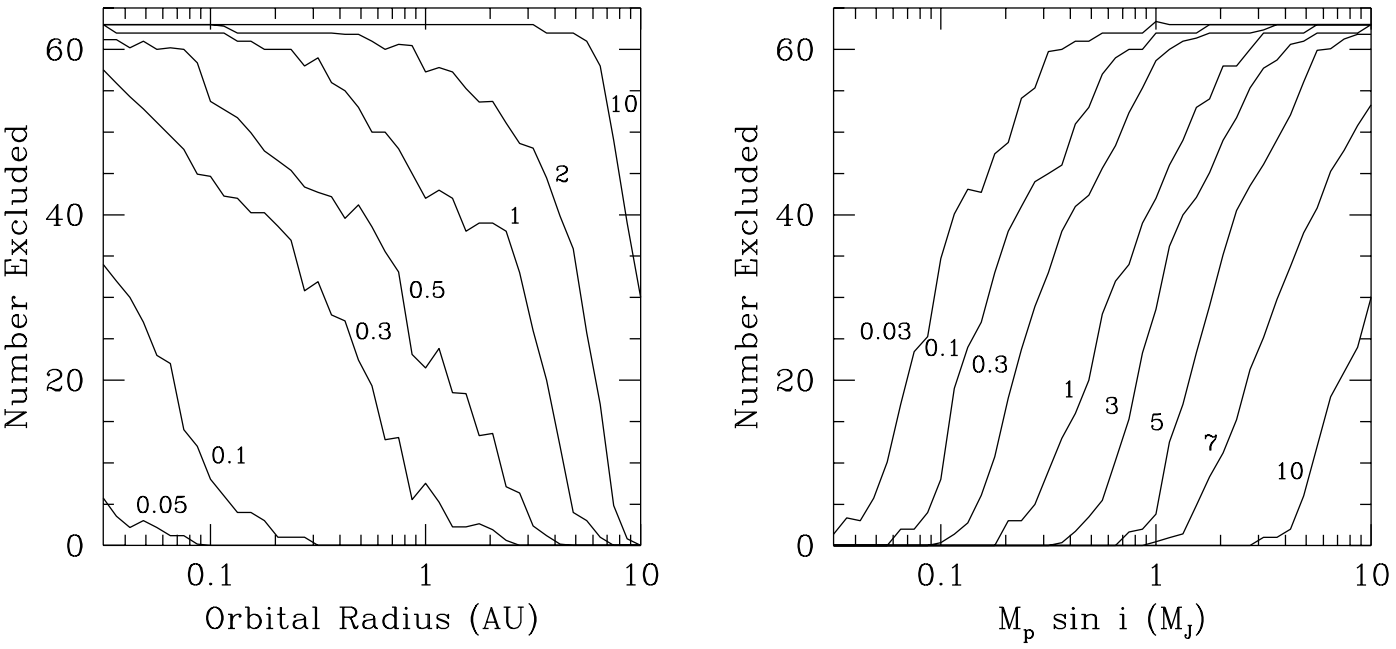

FIG. 10.—Number of stars from which a companion with a particular a and M_p sin i can be excluded at the 99% level. We show the number excluded as a function of a for different M_p sin i (*left-hand panel*) and as a function of M_p sin i for different a (*right-hand panel*). Each curve is a different section of the contour map of Fig. 9. The curves are labeled with the corresponding values of a or M_p sin i.

are statistically equivalent, and all three give a distribution of periodogram powers for Gaussian noise that is significantly different from the usually assumed exponential distribution (see Fig. 11). Unfortunately, it is not possible in general to write a simple analytic formula for the false alarm probability, making Monte Carlo methods essential.

Our results help to explain the observed distribution of mass and orbital radius of companions (see Fig. 6). The confirmed companions so far have velocity amplitudes $K > 40$ m s^{-1}, whereas the Doppler errors lie between 5 and 15 m s^{-1}. This is most likely because there is an effective detection threshold that comes about because of the ambiguity introduced by intrinsic velocity flutter (which may be periodic). Confirmation of an orbit is then difficult when the velocity amplitude is similar to the scatter predicted because of intrinsic variability and Doppler errors. We note, however, that in the chromospherically quiet stars ($P_{\rm rot} \gtrsim 14$ days), there are no candidate periodicities in the range 15–40 m s^{-1}. This may reflect a real paucity of companions in this range.

The finite duration of the observations makes it difficult to detect Jupiter-mass companions with orbital radius $a \gtrsim 3$ AU. Thus the four known companions with $a > 1$ AU may be only the first of a population of Jupiter-mass companions at large orbital radii. This is not true for more massive companions, however. It is striking that companions with $M_p \sin i > 3\ M_J$ are rare at orbital radii 4–6 AU; we could have detected such objects in $\sim$90% of stars, yet found none.

A few more years of observations will allow detection of Jupiter-mass companions at $a \sim 5$ AU, particularly as the poorer quality pre-fix observations become less important. Already, we are able to exclude velocity amplitudes of 10 m s^{-1} from 15% of the stars in the sample (for $a \lesssim 3$ AU). The velocity amplitudes that can be detected are ultimately limited by intrinsic stellar variability. Even for chromospherically inactive stars ($P_{\rm rot} \gtrsim 14$ days), there is intrinsic flutter of a few m s^{-1}. Detectability of short-period companions should improve in the future as there is more feedback between the observed variability and future observations (i.e., stars that show variability are observed more often). Care must be taken to include this effect in assessment of detectabilities.

Our analysis has assumed that the orbits of companions are circular. Yet eccentric orbits appear to be the norm for many of the planetary-mass companions (see Table 1 and Marcy et al. 1999). We find, however, that the periodogram gives a good estimate of the period for eccentric orbits. In addition, we do not expect our upper limits to change substantially for eccentric orbits, as we argued in § 4, except for long-period orbits for which eccentricities are important. The possibility of a nonzero eccentricity makes identification of an orbital period *impossible* for periods more than 2 or 3 times the duration of the observations. A possible extension of the periodogram to noncircular orbits would be to fit a Kepler orbit at each frequency and to define the periodogram power in terms of the χ^2 of the Kepler fit (see eq. [7]). It is not clear if the gain in detectability would outweigh the computing power needed for this nonlinear least-squares fit. A better approach may be to fit higher harmonics as suggested by Schwarzenberg-Czerny (1996).

The observed distribution of companions in mass and orbital radius shows a "piling-up" toward small orbital radii and a paucity of companions between orbital radii $a \sim 0.2$ AU and $a \sim 1$ AU. Because of the small number of companions in our sample, it is not possible for us to say whether these features are due to selection effects. Unfortunately, without knowledge of the detection thresholds of the other radial velocity surveys, we cannot include the other confirmed companions in our analysis. The candidate periodicities we find also show fewer candidates between $a \sim 0.2$ AU and $a \sim 1$ AU, which is intriguing. Future detections will show whether these features reflect the parent population of planetary-mass companions. It may be that companions are to be found at all orbital radii, or it may be that there are two populations of Jupiter-mass companions, one at orbital radii $a \lesssim 0.2$ AU and one at orbital radii $a \gtrsim 1$ AU.

Either scenario presents an interesting challenge to theorists. Orbital migration models have been proposed to explain the presence of giant planets at small orbital radii (Lin et al. 1999; Murray et al. 1998; Trilling et al. 1998; Ward 1997). These models naturally predict a "piling-up" at small orbital radii (Trilling et al. 1998) because the orbital migration timescale grows progressively shorter as the planet spirals inward. However, it is not clear exactly how such migration might be halted, in particular at orbital radii as large as 0.2 AU. Indeed, the inevitability of migration may be responsible for the low percentage of solar-type stars that have close planetary-mass companions (Ward 1997). If migration depends on gap formation, one would expect migration only to occur for companions above a certain mass. As yet, there is no observed dependence of the mass distribution on orbital radius, except for the lack of companions with $M_p \sin i \gtrsim 3$–$4\ M_J$ at large orbital radius, $a \sim 3$–5 AU.

There have also been suggestions that gravitational scattering of planets by other planets, companion stars, or neighboring stars in a young star cluster may play a role in determining the final distribution of orbital radii (Rasio & Ford 1996; Weidenschilling & Marzari 1996; Lin & Ida 1997; Laughlin & Adams 1998; Levison, Lissauer, & Duncan 1998). The large range of orbital eccentricities of the observed companions may be evidence for this type of scenario (Marcy et al. 1999). One way to lose enough energy to allow a planet to move from $\sim$5 AU to less than 1 AU may be interaction with the protoplanetary disk during the last stages of dissipation, as suggested by Marcy et al. (1999). It is not known to what extent these different physical mechanisms play a role in determining the distribution of planet masses and orbital radii. Clear theoretical predictions are needed if the discovery of more planetary mass companions is to allow us to distinguish between these different pictures.

We would like to thank Lars Bildsten, Debra Fischer, Evan Scannapieco, Jonathan Tan, and Andrew Youdin for useful discussions as this work progressed. Debra Fischer provided rotation periods for several stars, for which a program developed by Phil Shirts was used to measure the Ca IR triplet emission. Jeff Scargle and the referee, Andy Nelson, provided thoughtful comments on the manuscript. Alex Schwarzenberg-Czerny kindly provided a copy of his paper (Schwarzenberg-Czerny 1998). A. C. was partly supported by the Victor F. Lenzen Memorial Scholarship Fund at UC Berkeley. G. W. M. was partly supported by NSF grant AST 95-20443 and NASA grant NAGW-3182.

APPENDIX A

DERIVATION OF THE LOMB-SCARGLE PERIODOGRAM

In this section, we sketch the derivation of the traditional Lomb-Scargle formula from a least-squares fit of a sinusoid to the data and show how it relates to the floating-mean periodogram used in this paper. Following Lomb (1976), for each trial frequency $\omega = 2\pi/P$, our model for the velocities is

$$f_j(t_j) = A \cos \omega(t_j - \tau) + B \sin \omega(t_j - \tau) . \tag{A1}$$

The constant τ is introduced to simplify the calculation of χ^2, as the cross terms cancel if we choose τ such that

$$\sum w_j \sin \omega(t_j - \tau) \cos \omega(t_j - \tau) = 0 , \tag{A2}$$

or equivalently

$$\tan (2\omega\tau) = \frac{\sum w_j \sin 2\omega t_j}{\sum w_j \cos 2\omega t_j} . \tag{A3}$$

The best-fit values of the parameters A and B are those which minimize $\chi^2 = \sum w_j(v_j - f_j)^2$, where $w_j \propto 1/\sigma_j^2$ is the weight for data point j. Setting $\partial\chi^2/\partial A = 0$ and $\partial\chi^2/\partial B = 0$ and using equation (A2) gives

$$A = \frac{\sum w_j v_j \cos \omega(t_j - \tau)}{\sum w_j \cos^2 \omega(t_j - \tau)} ,$$

$$B = \frac{\sum w_j v_j \sin \omega(t_j - \tau)}{\sum w_j \sin^2 \omega(t_j - \tau)} . \tag{A4}$$

The amplitude K and phase ϕ of the sinusoid are obtained from $K^2 = A^2 + B^2$ and $\tan \phi = A/B$.

Using equation (A4) to substitute the best-fit A and B into $\chi^2 = \sum w_j(v_j - f_j)^2$, we find the minimum value of χ^2 at each frequency is

$$\chi^2_{\min}(\omega) = \sum w_j v_j^2 - \sum w_j f_j^2 , \tag{A5}$$

where f_j is now the best-fit sinusoid. As in § 3.3, we define the unnormalized periodogram power $\hat{z}$ as the reduction in the sum of squares (Lomb 1976),

$$\hat{z}(\omega) \equiv \sum w_j f_j^2 = \sum w_j v_j^2 - \chi^2_{\min}(\omega) , \tag{A6}$$

or

$$\hat{z}(\omega) = \frac{[\sum w_j v_j \cos \omega(t_j - \tau)]^2}{\sum w_j \cos^2 \omega(t_j - \tau)} + \frac{[\sum w_j v_j \sin \omega(t_j - \tau)]^2}{\sum w_j \sin^2 \omega(t_j - \tau)} . \tag{A7}$$

Equation (A7) is the (unnormalized) Lomb-Scargle periodogram (Lomb 1976; Scargle 1982; Horne & Baliunas 1986) modified for unequally weighted data (Gilliland & Baliunas 1987; Irwin et al. 1989; Scargle 1989). Equation (A6) shows that the floating-mean periodogram we adopt in this paper (§ 3.3) is a straightforward generalization of the traditional periodogram (see also Walker et al. 1995, eq. [A2]).

APPENDIX B

NORMALIZATION OF THE PERIODOGRAM AND THE DISTRIBUTION OF NOISE POWERS

There are three different prescriptions in the literature for normalizing the periodogram, namely dividing by (1) the sample variance (Horne & Baliunas 1986; Irwin et al. 1989; Walker et al. 1995), (2) the variance of the residuals to the best-fit sinusoid (Gilliland & Baliunas 1987; this paper), or (3) the variance of the residuals to the best-fit sinusoid *at each frequency* (Schwarzenberg-Czerny 1996). The motivation for these normalizations is to give the periodogram power z a simple statistical distribution when the data are pure noise. The goal is to assess the false alarm probability associated with a given periodogram power. Recent work by Schwarzenberg-Czerny (1997a, 1997b, 1998) has shown that all three normalizations are statistically equivalent, and, at a given frequency, each leads to a simple analytical distribution for Gaussian noise. We now expand on this discussion and describe our choice of normalization.

We point out that because of nonorthogonality between different frequencies, it is difficult to estimate the number of independent frequencies for a given data set. The commonly used empirical formula of Horne & Baliunas (1986) for the number of independent frequencies is based on an inaccurate probability distribution and is valid only for a particular frequency range. We stress that, unfortunately, it is not possible to write a simple analytic form for the false alarm probability, making Monte Carlo methods essential.

Why normalize the periodogram at all? Scargle (1982) and Horne & Baliunas (1986) showed that if the data points X_j are independent Gaussian deviates with variance σ_0^2, the distribution of unnormalized periodogram powers is

$$f(\hat{z})d\hat{z} = \frac{1}{\sigma_0^2} \exp\left(-\frac{\hat{z}}{\sigma_0^2}\right)d\hat{z} \tag{B1}$$

(or simply χ^2 with 2 degrees of freedom). This analysis extends to the weighted periodogram, where σ_0^2 is a measure of the overall normalization of the weights. We would like to stress that if the noise variance were somehow known in advance,[12] one could simply normalize by the known variance σ_0^2, thus obtaining

$$f(z)dz = \exp(-z)dz\ , \tag{B2}$$

an exponential distribution of periodogram powers. However, in many cases σ_0^2 is not known accurately in advance and must be estimated from the data. The idea is to normalize the noise powers to a known level,[13] aiding identification of localized features in the power spectrum (e.g., periodic signals).

To estimate the noise level from the data set, we use an "analysis of variance" approach (Schwarzenberg-Czerny 1989; Davies 1990). Equation (A6) shows that

$$\sum w_j v_j^2 = \hat{z}(\omega) + \chi^2_{\min}(\omega)\ . \tag{B3}$$

We now define

$$s^2 \equiv \frac{1}{N-m}\sum w_j v_j^2, \qquad s_f^2 \equiv \frac{\hat{z}}{2}, \qquad s_n^2 \equiv \frac{1}{N-m-2}\sum w_j(v_j - f_j)^2\ , \tag{B4}$$

and rewrite equation (B3) in terms of variances, giving

$$(N-m)s^2 = 2s_f^2 + (N-m-2)s_n^2\ . \tag{B5}$$

We have partitioned the variance into two pieces, together with their respective degrees of freedom; one piece from the signal s_f^2, and one piece from the noise s_n^2. Schwarzenberg-Czerny (1989, 1997a, 1998) showed that under the null hypothesis, s_n^2 and s_f^2 are statistically independent by Fisher's Lemma. This is also true if v_j consists of a sinusoidal signal plus Gaussian noise. In this case, s_n^2 is an unbiased estimate of the noise variance. The different definitions of the normalized periodogram are simply different ratios of the variances in equation (B5). The "traditional" normalization by the sample variance is $z \equiv s_f^2/s^2$, whereas normalizing by the residuals to the noise gives $z \equiv s_f^2/s_n^2$.

The distribution of powers when the X_j are independent Gaussian deviates can be written down analytically (Schwarzenberg-Czerny 1997a, 1997b). The partitioning of the degrees of freedom means that s^2, s_f^2, and s_n^2 are χ^2 distributed with $N-m$, 2, and $N-m-2$ degrees of freedom, respectively. Thus $z = s_f^2/s_n^2$ follows an F distribution with 2 and $N-m-2$ degrees of freedom (for example, see Abramowitz & Stegun 1971, § 26.6). The distribution of $z = s_f^2/s^2$ is more complex as s^2 is correlated[14] with s_f^2. The distribution of z in this case is an incomplete beta function (see Abromowitz & Stegun 1971, § 26.5). The probability that the periodogram power z is larger than a given value z_0 is given in Table 9 for the different normalizations.

Given a probability distribution for the periodogram power, we can write down an expression for the false alarm probability. If the probability that a periodogram power z is above some value z_0 is Prob $(z > z_0)$ (as in Table 9), then the false alarm probability is

$$F = 1 - [1 - \text{Prob}\ (z > z_0)]^M\ , \tag{B6}$$

where M is the number of independent frequencies that were examined. In Figure 11, we show the distribution of maximum periodogram powers for sets of evenly spaced data with $N = 20$. The crosses are the results of our Monte Carlo simulations.

TABLE 9

DISTRIBUTION OF PERIODOGRAM POWERS

Normalization Factor	Probability $(z > z_0)$[a]
σ^2	$\exp(-z_0)$
s^2	$1 - I_{2z_0/(N-m)}\left(1, \frac{N-m-2}{2}\right) = \left(1 - \frac{2z_0}{N-m}\right)^{(N-m-2)/2}$
s_n^2	$\int_{z_0}^{\infty} dz\ F_{2,N-m-2}(z) = \left(1 + \frac{2z_0}{N-m-2}\right)^{-(N-m-2)/2}$

[a] $I_x(a, b)$ is the incomplete beta function (Abramowitz & Stegun 1971); F_{ν_1,ν_2} is Fisher's F distribution with ν_1 and ν_2 degrees of freedom (Hoel, Port, & Stone 1971).

[12] This is often the situation in X-ray astronomy, for example, where the noise is dominated by Poisson photon statistics, giving a well-defined background power level (Leahy et al. 1983). See also the discussion in Lampton et al. (1976).

[13] As we noted in § 4.1, in principle, the background noise level in the power spectrum gives a direct measure of σ_0^2. However, in *practice*, the uneven sampling results in contamination of the noise powers by the signal because of spectral leakage and aliasing effects.

[14] This correlation was neglected by Koen (1990), who incorrectly presumed an F distribution in this case.

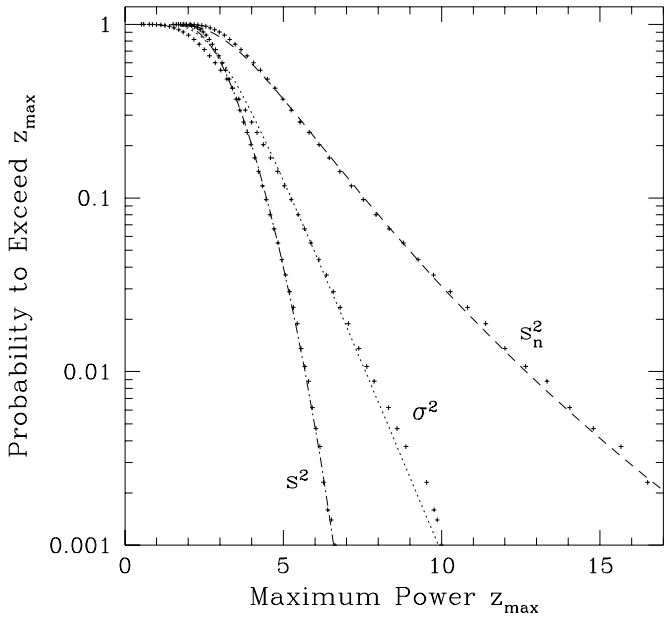

FIG. 11.—Distribution of maximum periodogram powers with different normalizations. The crosses are the results of Monte Carlo simulations. We generate ten thousand sets of $N = 20$ evenly spaced points drawn from a Gaussian distribution. The periodogram is evaluated at $2N$ evenly spaced frequencies between $1/N$ and $1/2$. Each curve is labeled with the normalization factor, either the known variance of the noise σ^2, the sample variance s^2 or the variance of the residuals s_n^2. Theoretical distributions are plotted as lines. The dotted line is the distribution $1 - [1 - \exp(-z)]^N$. The dashed and dot-dashed lines are of the form $1 - [1 - f(z)]^M$, where $f(z)$ is taken from Table 9. The best fit M was determined by fitting the tail of the F distribution (probability from 0.5 to 0.99), giving $M = 23.5$.

We used three different normalizations for the periodogram. The lines show the theoretical distributions. In the case where the noise variance σ_0^2 is known, we use equation (B6) with $\text{Prob}(z > z_0) = \exp(-z_0)$ and $M = N$ (*dotted line*). For the normalizations by s^2 and s_n^2 (*dot-dashed* and *dashed lines*), we use the distributions given in Table 9 and find the best-fit value of M, fitting to the tail (Prob > 0.5) of the distribution. Both distributions give the same value, $M = 23.5$. Notice that normalizing by s_n^2 broadens the distribution of maximum powers (because of the extra uncertainty in the value of s_n^2), whereas normalizing by s^2 narrows the distribution (because of the correlation with s_f^2).

Horne & Baliunas (1986) used Monte Carlo simulations to find the false alarm probability for evenly spaced data sets.[15] Normalizing by the sample variance, they assumed $\text{Prob}(z > z_0) = \exp(-z_0)$ and fit for M as a function of N. However, as Figure 11 shows, the distribution of z is different from exponential, especially in the tails of the distribution. *Thus the relations of Horne & Baliunas (1986) give inaccurate estimates of false alarm probabilities or detection thresholds.* Because the distribution is squashed, the effect is to *overestimate* both detection thresholds and false alarm probabilities.

In agreement with Press et al. (1992) and Marcy & Benitz (1989), Horne & Baliunas found that $M \approx N$ when the period range searched was from the average Nyquist period to the duration of the data set. However, in this paper, we evaluate frequencies several times larger than the average Nyquist frequency. A naive estimate of the number of independent frequencies is $T\Delta f$. Our numerical results show that in general the number of independent frequencies is less than this estimate; hence, our Monte Carlo approach for finding the false alarm probabilities in § 3.4. It would be useful to have a method, for a given data set, of estimating the number of independent frequencies, allowing one to write down false alarm probabilities analytically. One approach may be to look at the correlations between residuals (Schwarzenberg-Czerny 1991).

Finally, we discuss the difference between normalizing by s_n^2 at each frequency and normalizing by s_n^2 evaluated at the *best-fit* frequency. This choice is really a matter of taste. The distribution of maximum periodogram powers is the same, by definition. However, it seems to us that it is fairer to make comparisons between frequencies using the same normalization for the noise in χ^2. Thus our choice of normalization is that of Gilliland & Baliunas (1987, eq. [7]): we normalize by the same factor for each frequency, namely s_n^2 evaluated at the best-fit period.

[15] Note that due to a typographical error, the values of M given in the *tables* in HB86 are incorrect (S. L. Baliunas 1998, private communication).

REFERENCES

Abramovitz, M., & Stegun, I. 1971, Handbook of Mathematical Functions (New York: Dover)
Avni, Y. 1976, ApJ, 210, 642
Baliunas, S. L., Sokoloff, D., & Soon, W. 1996, ApJ, 457, L99
Beavers, W. I., & Salzer, J. J. 1983, PASP, 95, 79
Bevington, P. R., & Robinson, D. K. 1992, Data Reduction and Error Analysis for the Physical Sciences (2d ed.; New York: McGraw-Hill)
Black, D. C., & Scargle, J. D. 1982, ApJ, 263, 854
Brazier, K. T. S. 1994, MNRAS, 268, 709
Butler, R. P., & Marcy, G. W. 1996, ApJ, 464, L153
Butler, R. P., Marcy, G. W., Vogt, S. S., & Apps, K. 1998, PASP, 110, 1389
Butler, R. P., Marcy, G. W., Williams, E., Hauser, H., & Shirts, P. 1997, ApJ, 474, L115
Butler, R. P., Marcy, G. W., Williams, E., McCarthy, C., Dosanjh, P., & Vogt, S. S. 1996, PASP, 108, 500
Campbell, B., Walker, G. A. H., & Yang, S. 1988, ApJ, 331, 902
Carney, B. W., Latham, D. W., Laird, J. B., & Aguilar, L. A. 1994, AJ, 107, 2240
Cash, W. 1976, A&A, 52, 307
Caso, C., et al. 1998, European Phys. Journal, C3, 1
Cline, D., & Lesser, P. M. S. 1970, Nucl. Instrum. Meth., 82, 191
Cochran, W. D., & Hatzes, A. P. 1994, Ap&SS, 212, 281

Cochran, W. D., Hatzes, A. P., Butler, R. P., & Marcy, G. W. 1997, ApJ, 483, 457
Davies, S. R. 1990, MNRAS, 244, 93
de Jager, O. C. 1994, ApJ, 436, 239
Delfosse, X., Forveille, T., Mayor, M., Perrier, C., Naef, D., & Queloz, D. 1998, A&A, 338, L67
Eyer, L., & Bartholdi, P. 1998, A&AS, 135, 1
Ferraz-Mello, S. 1981, AJ, 86, 619
Fischer, D. A., Marcy, G. W., Butler, R. P., Vogt, S. S., & Apps, K. 1999, PASP, 111, 50
Gilliland, R. L., & Baliunas, S. L. 1987, ApJ, 314, 766
Hoel, P. G., Port, S. C., & Stone C. J. 1971, Introduction to Probability Theory (Boston: Houghton-Mifflin)
Horne, J. H., & Baliunas, S. L. 1986, ApJ, 302, 757
Irwin, A. W., Campbell, B., Morbey, C. L., Walker, G. A. H., & Yang, S. 1989, PASP, 101, 147
Irwin, A. W., Yang, S., & Walker, G. A. H. 1992, PASP, 104, 101
Kamper, K. W. 1987, AJ, 93, 683
Koen, C. 1990, ApJ, 348, 700
Lampton, M., Margon, B., & Bowyer, S. 1976, ApJ, 208, 177
Lang, K. R. 1991, Astrophysical Data (New York: Springer)
Latham, D. W., Mazeh, T., Stefanik, R. P., Mayor, M., & Burki, G. 1989, Nature, 339, 38
Laughlin, G., & Adams, F. C. 1998, ApJ, 508, L171
Leahy, D. A., Darbro, W., Elsner, R. F., Weisskopf, M. C., Sutherland, P. G., Kahn, S., & Grindlay, J. E. 1983, ApJ, 266, 160
Levison, H. F., Lissauer, J. J., & Duncan, M. J. 1998, AJ, 116, 1998
Lin, D. N. C., & Ida, S. 1997, ApJ, 477, 781
Lin, D. N. C., Papaloizou, J. C. B., Bryden, G., Ida, S., & Terquem, C. 1999, in Protostars and Planets IV, ed. V. Manning, A. Boss, & S. Russell, in press
Lomb, N. R. 1976, Ap&SS, 39, 447
Marcy, G. W., & Benitz, K. J. 1989, ApJ, 344, 441
Marcy, G. W., & Butler, R. P. 1992, PASP, 104, 270
———. 1996, ApJ, 464, L147
———. 1998, ARA&A, 36, 57
Marcy, G. W., Butler, R. P., Williams, E., Bildsten, L., Graham, J. R., Ghez, A. M., & Jernigan, J. G. 1997, ApJ, 481, 926
Marcy, G. W., Butler, R. P., Vogt, S. S., Fischer, D., & Lissauer, J. J. 1998, ApJ, 505, L147
Marcy, G. W., Butler, R. P., Vogt, S. S., Fischer, D., & Liu, M. 1999, ApJ, 520, 239
Marcy, G. W., Cochran, W. D., & Mayor, M. 1999, in Protostars and Planets IV, ed. V. Manning, A. Boss, & S. Russell, in press
Mayor, M., & Queloz, D. 1995, Nature, 378, 355
Mayor, M., Queloz, D., Beuzit, J.-L., Mariotti, J.-M., Naef, D., Perrier, C., & Sivan, J.-P. 1998, in Protostars and Planets IV, ed. V. Manning, A. Boss, & S. Russell, in press
McMillan, R. S., Moore, T. L., Perry, M. L., & Smith, P. H. 1994, Ap&SS, 212, 271
Murray, N., Hansen, B., Holman, M., & Tremaine, S. 1998, Science, 279, 69
Nelson, A. F., & Angel, J. R. P. 1998, ApJ, 500, 940
Noyes, R. W., Jha, S., Korzennik, S. G., Krockenberger, M., & Nisenson, P. 1997, ApJ, 483, L111
Press, W. H., Teukolsky, S. A., Vetterling, W. T., & Flannery, B. P. 1992, Numerical Recipes: The Art of Scientific Computing (2d ed.; New York: Cambridge Univ. Press)
Protheroe, R. J. 1987, Proc. Astron. Soc. Australia, 7, 167
Queloz, D., et al. 1999, preprint
Rasio, F. A., & Ford, E. B. 1996, Science, 274, 954
Saar, S. H., Butler, R. P., & Marcy, G. W. 1998, ApJ, 498, L153 (SBM98)
Saar, S. H., & Donahue, R. A. 1997, ApJ, 485, 319
Scargle, J. 1982, ApJ, 263, 835
———. 1989, ApJ, 343, 874
Schwarzenberg-Czerny, A. 1989, MNRAS, 241, 153
———. 1991, MNRAS, 253, 198
———. 1996, ApJ, 460, L107
———. 1997a, in Astronomical Time Series, ed. D. Maoz, A. Sternberg, & E. M. Leibowitz (Dordrecht: Kluwer), 183
———. 1997b, ApJ, 489, 941
———. 1998, Baltic Astron., 7, 43
Soderblom, D. R. 1985, AJ, 90, 2103
Tokovinin, A. A. 1991, A&AS, 91, 497
Trilling, D., Benz, W., Guillot, T., Lunine, J. I., Hubbard, W. B., & Burrows, A. 1998, ApJ, 500, 428
Vaughan, B. A., et al. 1994, ApJ, 435, 362
Walker, G. A. H., Walker, A. R., Irwin, A. W., Larson, A. M., Yang, S. L. S., & Richardson, D. C. 1995, Icarus, 116, 359 (W95)
Ward, W. R. 1997, Icarus, 126, 261
Weidenschilling, S. J., & Marzari, F. 1996, Nature, 384, 619